SALISH SEA
MARINE SURVIVAL PROJECT

LONG LIVE THE KINGS

PACIFIC SALMON FOUNDATION

# *Spatial temporal extent of bull kelp (Nereocystis leutkeana) floating canopy area on the west coast of Canada:*

*Development of a satellite mapping methodology with different spatial and spectral sensor characteristics and further evaluation for a large scale mapping project*

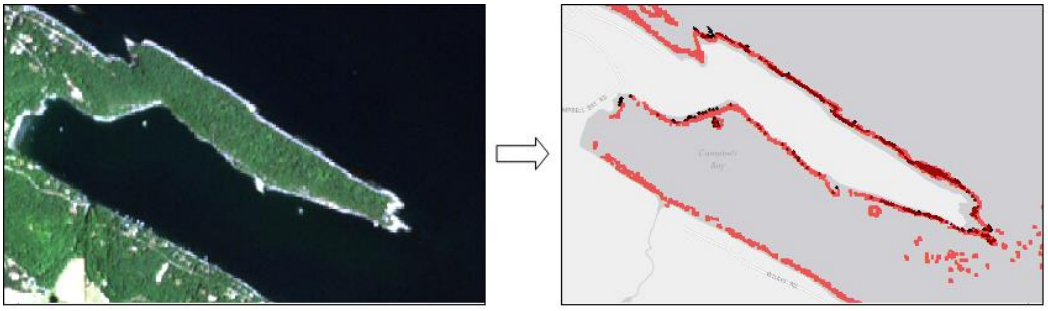


Executed by:
Jennifer D. O'Neill, M.Sc., Aquatic Biologist and Remote Sensing Scientist
Maycira Costa, PhD, SPECTRAL Lab, UVic

In collaboration with:
Leanna Boyer, SeaChange Marine Conservation Society, Mayne Island Conservancy Society
Stephen Phillips, M.Sc. student, UVic


September, 2015

# Spatial temporal extent of bull kelp (*Nereocystis leutkeana*) floating canopy area on the west coast of Canada: Development of a satellite mapping methodology with different spatial and spectral sensor characteristics and further evaluation for a large scale mapping project

## Summary of main findings:

This pilot study demonstrates the use of satellite optical imagery, specifically WorldView-2 and SPOT 6, to map the canopy distribution of kelp *Nereocystis leutkeana.* The best kelp map product attained in this study was produced from the SPOT-6 image, with the selected variable set of principle component PC2 and PC3 after image preprocessing steps of georectification, atmospheric correction, masking of land and depth below 30 m, and the statistical image processing steps of principle components analysis and variable reduction. The comparison of the satellite derived kelp map with the *in situ* kelp survey showed the high effectiveness of the developed procedures. It is important to highlight the difficultly in comparing satellite derived kelp maps with *in situ* survey data given (1) the mobility of kelp beds at the surface with changing water depth and current direction throughout tidal cycles; (2) the fast growth rate of *Nereocystis* rapidly changing the standing crop of kelp between the time of image acquisition and the time of kelp survey; (3) locational error intrinsic in field surveys due to occasional human error, the accuracy level of the GPS, and availability of satellites to the GPS unit; and (4) full characterization of the reflectance of what could be false-positives.

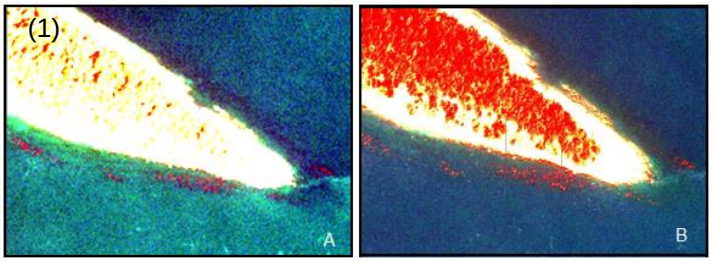


*(1). A subset of WorldView-2 image (a) before and (b) after pan-sharpening technique. Note the improvement in spectral resolution and improvement in visual detection of the fringing kelp (red) around the island. The kelp and the vegetation on the island appear as red because the NIR band is placed in the red colour. (Display bands are NIR/G/B).*

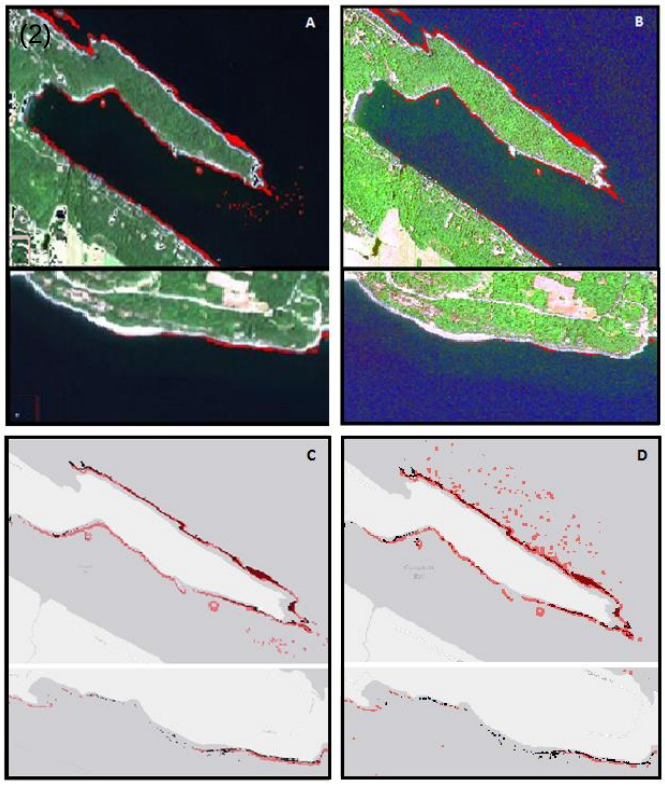


*(2).Classification results for the SPOT-6 PC2 & PC3 (a) before and (b) after pan-sharpening transformation to increase spatial resolution. The kelp classification is shown in red, while the ground truth survey kelp distribution is shown in black (c,d).*

## I. Introduction

At present, kelp mapping is conducted manually via transects and aerial photography (Cavanaugh et al., 2010; Sutherland et al., 2007; Field, 1996). In British Columbia, the Ministry of Environment has conducted kelp surveys in allocated areas along the coast since the 70's using field transects and infrared aerial photos (Sutherland, 1990; Sutherland et al., 2007; Lucas et al., 2007). Localized kelp inventory initiatives have also been established recently in the Gulf Islands area, such as through the Mayne Island Conservancy Society and the citizen science group Help the Kelp on Gabriola Island (Mayne Island Conservation Society, 2010; Help the Kelp, 2015).

Though effective, on-the-ground kelp survey strategy suffers the fallbacks of labour and time-intensiveness and is limited solely to accessible areas. Because the issues affecting kelp and the biota that utilize it, such as climate change, are broad scale and time sensitive the need for ancillary mapping and monitoring strategies is growing. Optical remote imagery has been proposed as one such supplementary method, as it can capture data from large and inaccessible areas cost- and time- effectively, nearly instantly, with high frequency, and with the potential for automation (Simis and Duboi, 2001; Cavanaugh et al., 2010; Cavanaugh et al., 2011; Casal et al., 2011). Additionally, there is potential for historical distribution of kelp to be derived from historical imagery as far back as 1986 with the launch of the SPOT satellite series. Given the development of proper methodology for retrievals of kelp canopy extent, satellite imagery could be used to reveal the spatial temporal dynamics of the kelp ecosystem. The need of *Nereocystis* maps was one of the main outcomes of the Pacific Salmon Foundation's Salmon Habitat Meeting in July 2014.

In the peer reviewed literature, headway has been made in remote mapping of the kelp species *Macrocystis integrifolia* on the west coast USA (Cavanaugh et al., 2010; Cavanaugh et al., 2011). However, literature on the remote mapping of *Nereocystis leutkeana* is sparse. Its differing morphology and its formation of characteristically smaller beds pose unique challenges for identifying *Nereocystis* in imagery. This pilot project aims to (1) identify the unique spectral bands, spatial resolution, and contextual information that characterize *Nereocystis* beds and (2) develop image processing methodologies best suited for integrating these identifiers in satellite imagery to map the aerial extent of *Nereocystis* beds in BC coastal waters.

A remote optical sensor's ability to identify kelp beds, such as *Nereocystis* and *Macrocystis*, relies mostly on the high reflectance in the infrared spectra compared to very low reflectance from the water (Cavanaugh et al., 2010; Cavanaugh et al., 2011). Water strongly absorbs light in the infrared spectra due to the vibrational process on the water molecules. On the other hand, floating kelp strongly reflects infrared radiation due to the interaction of infrared light within the cell structure of the kelp. Figure 1 illustrates the different spectral properties of optically deep water and kelp. Note that the curve is for the kelp species *Macrocystis integrifolia* and not *Nereocystis leutkeana*; however, a similar vegetation curve is expected for both kelp species when floating at the surface. The visible bands may also play a role in the detection of kelp. Kelp exhibits a characteristic reflectance peak in the green and red wavelength ranges due to the presence of photosynthetic pigments chlorophyll-a and fucoxanthin, respectively. Research has demonstrated that variance in the SPOT-5 red band can denote the presence of kelp (Cavanaugh et al., 2010). Detection will therefore depend on the spectral resolution and sensitivity of the sensor in the visible and NIR wavelengths.

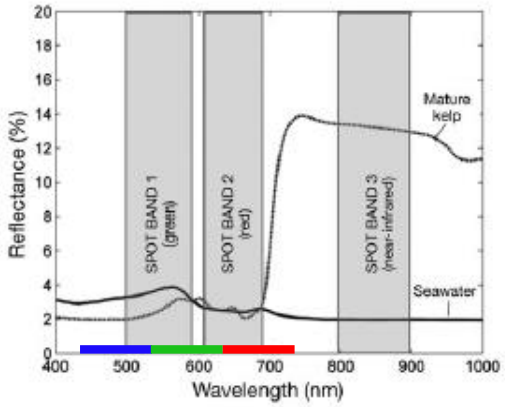


*Figure 1. Spectral signature of kelp versus optically deep water (modified from Cavanaugh et al., 2010).*

A remotely sensed image, especially one acquired from space, is an optical puzzle. The spectral signatures of kelp (the target signal) and all other benthic cover classes in an image are complicated by the attenuating effects of the atmosphere, water surface, water constituents, and the water itself (Kirk, 1994). Each of these physical media absorbs and reflects light in unique ways, and as a result, adds noise into the image. In other words, reflectance peaks and absorption troughs from the overlying ocean and atmosphere are incorporated into the target spectra of kelp, obscuring its unique signal. Image pre-processing techniques such as atmospheric correction and surface glint removal must be applied to compensate for these effects prior to classification (Maritorena et al., 1994; Hedley et al., 2005).

Detection of kelp beds also depends on the spatial resolution of the satellite sensor. Previous studies have had success mapping the larger bed-forming Giant Kelp (*Macrocystis integrifolia*) with 10 m resolution SPOT-5 imagery and even 30 m resolution Landsat imagery (Cavanaugh et al. 2010;2011, Byrnes et al., 2011). Little literature has been published on the remote mapping of bull kelp *Nereocystis leutkeana*. Its differing morphology (thin and tubular with large floating bulbs and fronds, versus the branching, diffuse fronds spread through the water column of Giant Kelp) and its formation of characteristically smaller beds pose unique challenges for remote identification. *Nereocystis* often forms linear fringing beds 4-5 metres wide and occurs in patches of 4-5 metres diameter. This study addresses the question of optimal spatial resolution by determining which resolution, of available data, is sufficient to resolve the smaller bed morphology. The available testing resolutions are SPOT-6 6m and 1.5m data and WorldView-2 2m and 0.5m pixel sizes.

## II. Objectives

The present study is a pilot project aiming to evaluate and define methodologies for using satellite imagery to map the aerial extent of bull kelp (*Nereocystis leutkeana*) beds in British Columbia coastal waters. The long-term goal is to apply the developed methods to B.C. coastal waters and work together with local communities and First Nations in collaboration with marine conservation organizations and government agencies to improve data collection and the use of satellite imagery. At present, the majority of kelp mapping is conducted manually via transects and aerial photography. Though effective, the strategy is labour-intensive, requires large time investment, and is limited by the areas accessible to survey.

## III. Methods

### A. Study Site:

Mayne Island is situated in the Southern Gulf Islands between Vancouver and Victoria, British Columbia, within the Strait of Georgia (Figure 2). *Nereocystis* beds are found in the many rocky bays and fringing reefs around the island, while eelgrass forms both flat and fringing beds in several shallow sandy bays. The Mayne Island Conservation Society together with SeaChange Marine Conservation Society, have been mapping the eelgrass distribution from 2008 to present and the kelp distribution from 2010 to present in select areas via citizen science community mapping efforts (MICS, 2010).

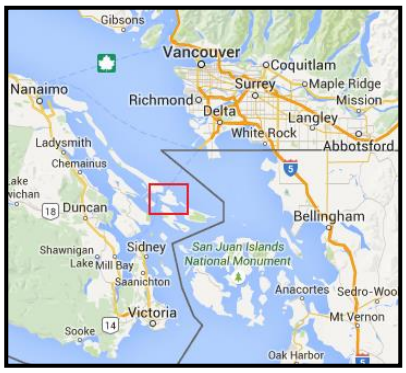


*Figure 2. Location of pilot study site, Mayne Island, within red box.*

### B. Data:

A WorldView-2 image was acquired from the Digital Globe historical image archive for August 1, 2013 over Mayne Island (Figure 3a). The image was chosen from during the months of July through September when kelp canopies were fully developed and as close as possible to a nadir view and solar noon; Tide level was as close to low tide as possible (1.36 m). Spatial resolution of the WorldView-2 multispectral (colour) image is 2.0m, and the panchromatic (greyscale) image is 0.5 m.

A SPOT6 image was acquired from the CNES historical image archive for July 26, 2014 over Mayne Island (Figure 3b). The image was chosen from during the months of July through September when kelp canopies were fully developed and as close as possible to a nadir view and solar noon; Tide level was as close to low tide as possible (0.69m). Spatial resolution of the SPOT6 multispectral (colour) image is 6.0 m, and the panchromatic (greyscale) image is 1.5 m. The ancillary parameters of each image dataset are listed in Table 1.

*Figure 3. Historical archived remote imagery data acquired for the present study over Mayne Island by satellite sensors (a) WorldView-2 (multispectral/panchromatic spatial resolution 2.0m/0.5m and 8 spectral bands) acquired on August 1, 2013 and (b) satellite sensor SPOT-6 (multispectral/panchromatic spatial resolution 1.5m/6.0m and 4 spectral bands) acquired on July 26, 2014. Displayed bands are RGB.*

*Table 1: Satellite imagery acquired for Nereocystis remote mapping feasibility study*

| Sensor | Month | Year | Tide (m) | spatial resolution of multispectral / panchromatic images (m) | spectral resolution (no. bands) |
|---|---|---|---|---|---|
| WorldView-2 | Aug | 2013 | 1.36 | 2.0 / 0.5 | 8 |
| SPOT-6 | July | 2014 | 0.69 | 6.0 / 1.5 | 4 |

Multibeam bathymetry with a horizontal spatial resolution of 25 m and vertical resolution of 1 m data was acquired from Parks Canada, Gulf Islands National Park of Canada.

Ground-truth data for classification training and product validation were compiled from spatial data archives of the Mayne Island Conservation Society (MICS). MICS conducts annual kelp and eelgrass distribution surveys around Mayne Island with the help of volunteer stewards from the local community. Kelp extent data was collected using a hand held Global Positioning System via kayak. Kelp waypoint data was delineated in three categories based on proximity and formation as outlined in the '*Guidelines and methods for mapping and monitoring kelp forest habitat in British Columbia*,' document generated by the Mayne Island Conservancy Society (MICS, 2010). (1) Point data represented solitary bulbs less than 5m in diameter and at a distance greater than 8m from other bulbs or clusters; (2) Line data represented bulbs that formed solitary lines where each bulb was no greater than 8m distance from the others or where lines were less than 5m in width; (3) Polygon data represented kelp beds greater than 5m across and maintained by less than 8m between bulbs. Variances in distance or width resulted in the end point of a polygon (bed) and the start of a new point, line or polygon. Different portions of the island were surveyed in different years. In 2013, the year that the WorldView-2 image was acquired, Kelp Survey Area 6 around Georgeson Island and Survey Area 9 around Curlew Island were acquired. In 2014, the year that the SPOT-6 image was acquired, Kelp Survey Areas 3, 4 and 5 around Edith Point and the north portion of Campbell Bay and Survey Area 11 along a portion of Navy Channel were acquired (MICS, 2015a) (Figure 4).

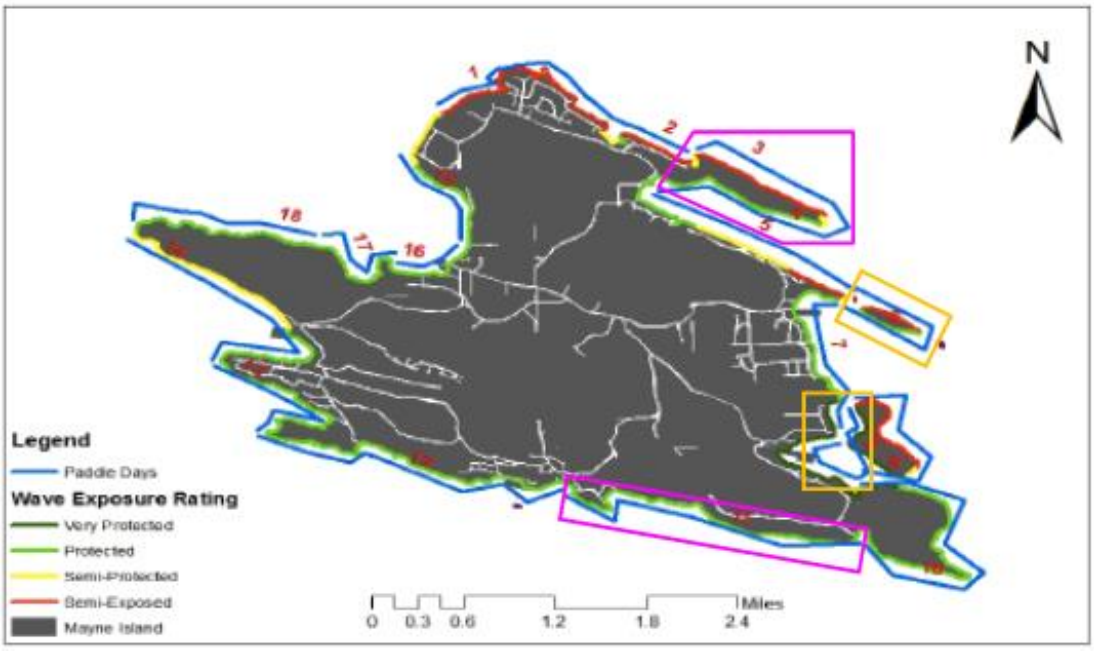


*Figure 4. Mayne Island Conservation Society monitoring schedule for Mayne Island Bull Kelp. The 2013 survey sites, outlined in orange, were Areas 6 (Georgeson Island) and 9 (West Curlew Island) and provide ground truth for the WorldView-2 image. The 2014 survey sites, outlined in magenta, were Areas 3, 4 and 5 (Edith Point and north Campbell Bay) and 11(a portion of Navy Channel) and provide ground truth for the SPOT6 image. Adapted from MICS (2015a).*

## C. Image pre-processing

*Radiometric calibration, atmospheric correction, and masking*

The WorldView-2 and SPOT-6 multispectral and panchromatic images were each mosaicked from original tiles with nearest neighbour resampling, radiometrically calibrated to convert them from raw digital numbers to at-sensor radiance, and then atmospherically corrected using the FLAASH radiative transfer model implemented in ENVI. The resulting reflectance image for WorldView-2 contained a large amount of complex haze. The haze was minimized using single image normalization by histogram adjustment (Jensen, 1996) where the minimum reflectance value was subtracted from the entire histogram for each band independently. This method set the minimum value of each band to zero while maintaining histogram distribution, thereby reducing haze, but maintaining the spectral relationships of the ground covers. The SPOT-6 image did not contain haze effects and therefore was not normalized with histogram adjustment.

Last, each image was geometrically corrected to a common datum so that the kelp survey data used for training WV-2 and SPOT classifications would fall in precisely the same locations on both images. The georectification was carried out by establishing ground control points (GCPs) over recognizable temporally stable landmarks such as road intersections, corners of buildings and lighthouses in both the image to be georectified (WV-2 or SPOT) and a geometrically correct aerial photograph of Mayne Island. The WV-2 and SPOT images were then warped to match the aerial photo. Root mean square error (RMSE) values were 0.56 pixels for the WV-2 image and 0.58 pixels for the SPOT-6 image.

*Masking land and cloud – WorldView-2*

A land mask was created for the WorldView-2 image by masking the following parameters, and then applying an erode filter with a 5x5 pixel window and manually masking any inland bodies of water that were not captured by the spectral mask.

$$R_{rs}^{+}{}_{(833nm)} > 0.2\ sr^{-1} \quad (1)$$

$$R_{rs}^{+}{}_{(833nm)} : R_{rs}^{+}{}_{(608nm)} > 0.25 \quad (2)$$

$$NDVI > 0.67 \quad (3)$$

$$\text{Where } NDVI = [R_{rs}^{+}{}_{(833nm)} - R_{rs}^{+}{}_{(659nm)}] / [R_{rs}^{+}{}_{(833nm)} + R_{rs}^{+}{}_{(659nm)}] \quad (4)$$

where $R_{rs}^{+}{}_{(833nm)}$ is the above water remote sensing reflectance in band 7 (NIR band centred at 833nm), $R_{rs}^{+}{}_{(608nm)}$ is the reflectance in band 4 (yellow band centred at 608nm), and $R_{rs}^{+}{}_{(659nm)}$ is the reflectance in band 5 (red band centred at 659nm).

A low altitude cloud mask was defined similar to Montes et al. (2004) using an NIR threshold values, but modified as follows:

$$R_{rs}^{+}{}_{(427nm)} > 0.07\ sr^{-1} \quad (5)$$

$$R_{rs}^{+}{}_{(949nm)} = 0.012\text{-}0.120\ sr^{-1} \quad (6)$$

$$R_{rs}^{+}{}_{(546nm)} / R_{rs}^{+}{}_{(478nm)} < 0.8 \quad (7)$$

$$NDVI < 0 \quad (8)$$

where $R_{rs}^{+}{}_{(949nm)}$ is the above water remote sensing reflectance in band 8 (NIR band centred at 949nm).

*Masking land, cloud – SPOT-6*

A land mask was created for the SPOT-6 image by masking the following parameters and manually masking any inland bodies of water that were not captured by the spectral mask.

$$DN_{(band4,825nm)} > 500 \quad (9)$$

where $DN_{(825nm)}$ is the above water raw digital number in band 4 (NIR band centred at 825nm).

The SPOT-6 image was free of low altitude clouds and therefore a cloud mask was not necessary.

*Masking lower kelp depth limit – WorldView-2 and SPOT-6*

A depth mask was developed to restrict further image analysis to areas of known kelp habitat. The mask was defined using the bathymetry dataset with a range of 0 m to 30 m since *Nereocystis* is known to inhabit depths of up to 30 metres (Springer et al., 2007).

*Surface glint correction – WorldView-2 and SPOT-6*

Surface glint correction was applied using the methods of Hedley et al. (2005), which use the infrared reflectance of optically deep water in the image to interpolate and remove glint reflectance in the visible range for the entire image. Mathematically,

$$R_{rs}'_{(i)} = R_{rs}^{+}{}_{(i)} - b_{(i)} \times [R_{rs}^{+}{}_{(NIR)} - \min R_{rs}^{+}{}_{(NIR)}] \quad (10)$$

where $R_{rs}'_{(i)}$ is above water remote sensing reflectance in visible band i for a pixel that is glint corrected; $R_{rs}^{+}{}_{(i)}$ and $R_{rs}^{+}{}_{(NIR)}$ are above water remote sensing reflectance in visible band i and an NIR band respectively, for the initial non-glint-corrected pixel; $b_{(i)}$ is the proportionality factor defined as the slope of the linear regression between the reflectance at visible band i and the NIR band within regions of variously sun glinted optically deep water; min $R_{rs}^{+}{}_{(NIR)}$ is the minimum NIR reflectance value found in the entire image and represents a pixel containing zero sun glint (Hedley et al., 2005). Because this method assumes the water-leaving NIR signal is zero, pixels containing floating vegetation such as kelp were masked out before glint correction to avoid over-correction. The floating vegetation mask was created by masking the following parameters,

$$\text{WorldView-2:} \quad NDVI > 0.254 \quad (11)$$

$$\text{SPOT-6:} \quad NDVI > 0.200 \quad (12)$$

and then applying a smoothing filter with a 5x5 and 3x3 pixel window for WV-2 and SPOT-6 respectively to include single or small clusters of pixels in the middle of kelp beds in the mask.

## D. Image processing

*Benthic classes*

Benthic substrate classes were defined as: kelp, sand, eelgrass, green algae, and deep water (>15m depth). Four total cases of kelp/other substrate class pairing were defined as kelp/sand, kelp/eelgrass, kelp/green algae, and kelp/deep water.

***Case 1:*** *Reflectance bands and band ratios with variable selection*

For each image, WV-2 and SPOT-6, the ratios between each band pair were calculated (e.g. band1:band2, band4:band7), which yielded eight reflectance bands and 28 reflectance band ratios (together termed 36 spectral variables) for the WV-2 image; and yielded four reflectance bands and six reflectance band ratios for the SPOT-6 image (together termed 10 spectral variables).

In the next step, the reflectance/ratio band pool for each image was reduced to only those bands which most effectively separated kelp from the other benthic classes. This reduction improved classification by eliminating redundancy and reducing the amount of noise in the image. To reduce the variable set and determine the best bands for separating kelp from the other benthic classes, the M-statistic was employed (Equation 13). The M-statistic is a measure of class separability. It normalizes the difference between the means of two benthic classes ($\mu_{1(\lambda)} - \mu_{2(\lambda)}$) by the sum of their standard deviations ($\sigma_{1(\lambda)} - \sigma_{2(\lambda)}$) at a specified variable, as follows (Kaufman and Remer, 1994):

$$M(\lambda) = \frac{\mu_{1(\lambda)} - \mu_{2(\lambda)}}{\sigma_{1(\lambda)} - \sigma_{2(\lambda)}} \quad (13)$$

A large M-statistic indicates good separation between the two classes because within-class variance is minimized and between-class variance maximized. Following Kaufman and Remer (1994), and M-statistic greater than 1.0 is defined as good class separation and an M-statistic lesser than 1.0 indicates poor separation. Since the M-

statistic in this study assessed separability for each benthic class pair independently, it offered the benefit of focusing only on the separability of benthic class pairs involving kelp, and ignoring non-kelp pairs. This ensured definition of the highest separability of kelp without including spurious variables that are useful for separating other non-kelp variables.

For each kelp/other benthic class pair (see benthic classes, directly above) independently, the M-statistic was calculated at each variable in the initial set of spectral variables (28 for WV-2 and 10 for SPOT6). The variable with the greatest M-statistic value (i.e. the variable yielding greatest spectral separation) was identified for each kelp/other substrate pair. Each of these greatest M-statistic values, provided it was greater than 1.0, was retained in the "Case 1 selected variable set," which by definition yields the greatest spectral separation between kelp and the other benthic classes with the least redundancy and noise, and therefore yield the most accurate classification.

***Case 2:*** *Principle components analysis with variable selection*

Principle Components Analysis (PCA) was applied to each image as an alternative technique to enhance the detection of kelp. PCA takes multiple variables and rearranges them into uncorrelated variables, termed principle component bands (PCs). The result is a set of PC bands, where each PC represents a combination of original image bands. The first PC band accounts for as much of the total image variance as possible, the second PC band accounts for as much of the remaining variance as possible, and so on down to the last PC band. The PCA was carried out to (1) define key bands for which variance denotes kelp presence and (2) remove spectral noise unrelated to kelp presence. Although spectral noise is often contained in the last few PC bands, this is not a steadfast rule. Nor will kelp variance always be contained in the first variable. For this reason, after PCA was performed, variable selection was carried out on the total set of PC bands in the same manner as in Case 1 to yield the "case 2 selected variable set."

***Case 3:*** *Panchromatic Image Sharpening*

To access the highest possible spatial resolution of the satellite sensor, the higher spatial resolution panchromatic (greyscale) band can be merged with the lower spatial resolution multispectral (colour) bands in a process called panchromatic sharpening, or pan-sharpening. This merging of the bands increases the spatial resolution of the lower multispectral resolution to the higher panchromatic resolution (2m to 0.5m in the case of WorldView-2 and 6m to 1.5m in the case of SPOT-6). Gram-Schmidt panchromatic sharpening transformation was performed on the best selected variable set to test whether the improvement in spatial resolution offered improvement in the kelp mapping accuracy. It is hypothesized that a finer image spatial resolution may more closely match the scale of spatial variance of kelp beds, thereby decreasing within-pixel heterogeneity, and improving the classification accuracy.

## E. Classification

One spectral variables selection was complete for Cases 1 and 2, the selected bands were compiled and merged into a single image for each case. A classification was then applied to each image. The purpose of a classification is to determine a benthic cover class for each pixel. The benthic cover class assigned to a pixel is the cover class that is deemed most likely, given the spectral character of each benthic class. The classification algorithm used in this study was the Maximum Likelihood classifier. The Maximum Likelihood classifier uses linear discriminant functions to calculate the probability of an unknown pixel belonging to each class and then

assigns the pixel to the class of highest probability (Richards, 1999). This algorithm is a supervised classifier, meaning ground truth information is provided by the analyst to train the algorithm. The algorithm is trained to recognize each cover class by assigning training regions of interest (ROIs) to known locations of each class from ground truth surveys, taking care to encompass the spectral range of each cover. The algorithm then views each pixel one by one and matches its spectrum to the average spectrum of the provided ROIs for each cover class. The cover class which is the best spectral match to the pixel's spectrum is assigned to that pixel.

Twenty percent of all ground truth data were assigned as training data by random sampling of the surveyed sites. The point, line, and polygon ground truth shape files were converted to vector format, overlain on the image in ENVI, converted to raster format (pixels), and then split through random sampling into 20% and remaining 80% subsamples. Using the statistical information from the 20% of ground truth pixels (termed training ROIs), the Maximum Likelihood classification algorithm assigned the each pixel in the image to the benthic class of the closest spectral match. Each classification output was treated with a sieve filter to eliminate speckle before validation (Macleod and Congalton, 1998).

**F. Validation**

Validation was performed by (1) comparing the kelp class designated by classification to the true substrate at that location as determined in the field and (2) comparing the visual distribution of the kelp between ground data maps and the satellite image maps. For (1) the remaining 80% subset of the MICS ground truth survey data was used as validation data (termed testing ROIs). A typical validation matrix was then constructed to calculate producer accuracy for a given kelp map. Producer accuracy is defined as the percentage of kelp testing ROIs that were classified correctly, or in other words, how well the testing ROIs were classified, and an indication of omission errors or "false negatives" (Story & Congalton, 1986; Guild et al., 2004).

The mathematical validation process, however, yields false classification errors under specific conditions. These conditions are the periodic mismatch between kelp surveys and image acquisition for the following variables: date, time, tide, and kelp distribution. The ground truth kelp surveys and image acquisition occurred in the same year and within the kelp growing season (July through September) but occurred on different dates, times, and tidal stages. The consequence of a mismatched date is such that if the ground truth survey occurs earlier in the kelp growing season than image acquisition, there will be more kelp present in the image than in the ground truth distribution, and commission error (false positives) will be introduced. If the ground truth survey occurs closer to peak kelp growth than the image acquisition does, there will be less kelp present in the image than in the ground truth distribution, and omission error (false negatives) will be introduced. Similarly, omission and commission error can both occur when the kelp surveys and remote image were acquired at different tidal heights. Due to the length and flexibility of the kelp stipe, the *Nereocystis* bulbs can drift a distance on the surface that is proportional to the change in water depth. For this reason, the producer errors are a less representative measure of map accuracy than the visual distribution of the kelp classifications. Producer errors were calculated and reported in this study, but the comparison of visual distribution of the kelp between ground data maps and the satellite image maps was considered with greater weight.

For (2), the comparisons between ground data maps and satellite image classifications were made by overlaying the polygons of each kelp map product over the polygons, lines and points generated by the ground truth kelp surveys. The visual comparison were made by assessing the kelp map for a match to the ground truth kelp survey map in terms of general location, shape, area, and environmental context. For example a linear kelp

bed which is the same size and length as the kelp ground truth survey map, but skewed four metres to the west would be considered a good match even though not directly overlapping due to the context of tidal drift over time.

## IV. Results and Discussion

### A. Image pre-processing

*Radiance conversion and atmospheric correction*

The image data was converted from raw DN numbers into radiance (Figure 5a) and then atmospherically corrected (Figure 5b) and haze corrected (Figure 5c) to remove effects of the atmosphere. Figure 5 depicts the spectral effect of the processes on a pixel containing vegetation in the WorldView-2 image. After conversion from DN to radiance, the image has exaggerated radiance values in the shorter wavelengths, particularly the blue to green range (0.4-0.6µm) and relatively lesser values in the NIR range (0.8-0.9µm) (Figure 5a). After atmospheric correction, the radiance values in the blue range are decreased and the NIR values increased to more realistic on-the-ground values (Figure 5b). Because the atmospheric correction does not account for the presence of haze in the image, the blue range still remains high (a vegetation signature characteristically has lower blue radiance than green due to absorption by chlorophyll pigments in the blue range). After haze correction, the reflectance of the blue range has been reduced to expected relative values (Figure 5c).

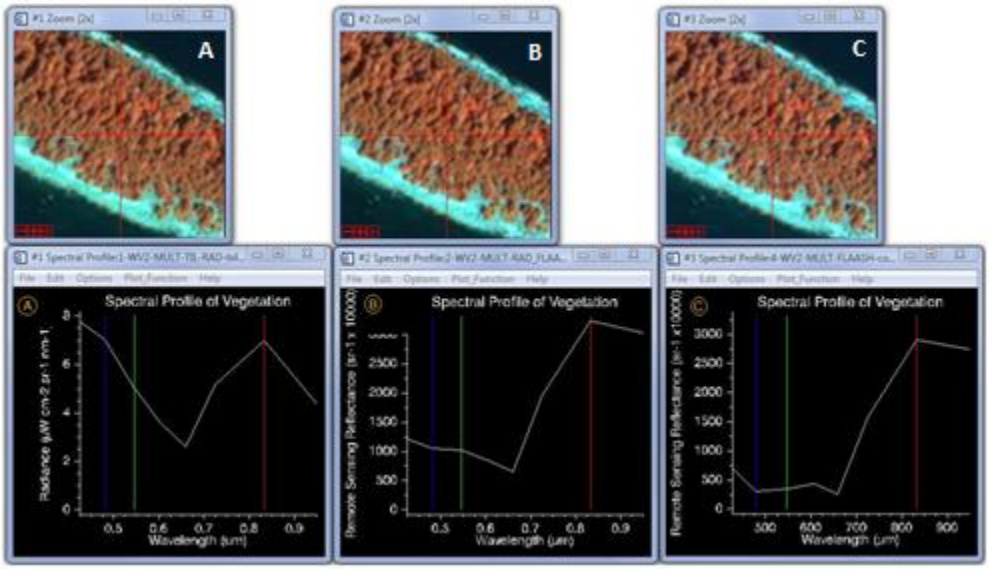


*Figure 5. Preprocessing steps for WorldView-2 image, as demonstrated on a single pixel containing vegetation. (a) Initial sensor radiance; (b) atmosphere corrected reflectance (note removal of atmospheric reflectance in the blue bands at 0.5 to 0.6µm and the change of units); and (c) haze correction (note further reduction of atmospheric blue reflectance and clearer green reflectance peak characteristic of vegetation at 550-600nm). The pre-processing steps removed unnecessary atmospheric noise with the effect of uncovering the characteristic spectra of cover classes.*

*Image masking*

A land mask, cloud mask, and mask for kelp depth limit of growth were built for the WorldView-2 image. The SPOT image was cloud free and therefore required only a land mask and a mask for kelp depth limit of growth. Figure 6 illustrates the land, cloud, and 30 m depth limit masks developed for the WorldView-2 image.

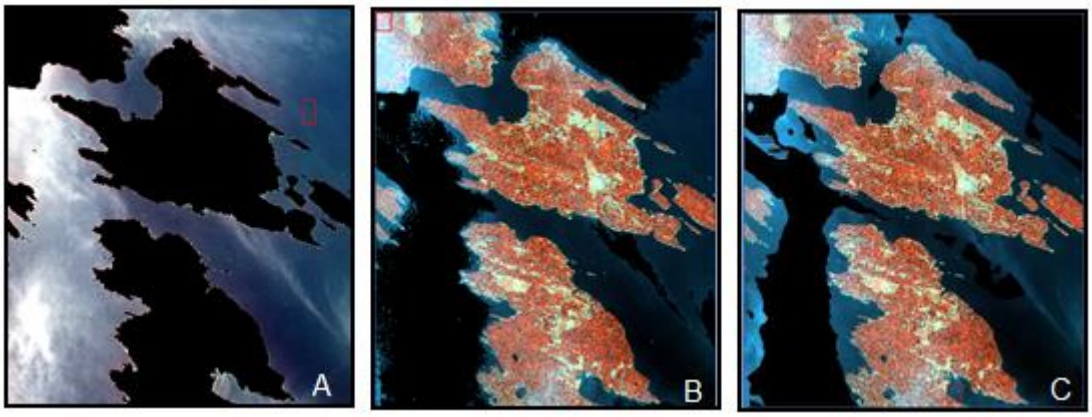


*Figure 6. (a) Land mask; (b) cloud mask; and (c) mask for lower depth limit of kelp for the WV-2 image.*

*Surface glint correction*

A surface glint correction was applied to the imagery using the method of Hedley et al. (2005). The correction improved visibility in some areas (Figure 7), however the results were skewed by the presence of cloud and haze. The glint correction method used the infrared reflectance of optically deep water in the image to interpolate and remove glint reflectance in the visible range for the entire image. At the same time, residual cloud and haze contributed noise in the same NIR range. The result is that after glint correction, the NIR range exhibited a very high variance due to over-correction of glint in hazy areas (Figure 8). Since this high NIR variance would bias the principle components analysis, the surface glint correction was not retained during further processing. The impact of removing the glint correction is low, given that glint correction improves the detection of submerged substrates. The majority of detectable kelp is floating, and that which is submerged, is shielded from glint-causing wave action by the buffering effects of the kelp bed. Even submerged eelgrass at Mayne Island is relatively void of glint-causing wave action due to its occurrence in sheltered bays. Bennett Bay, Campbell Bay, Horton Bay and the area surrounding Curlew Island contain the majority of visible eelgrass habitat unobstructed by cloud, and all are sheltered from wave action.

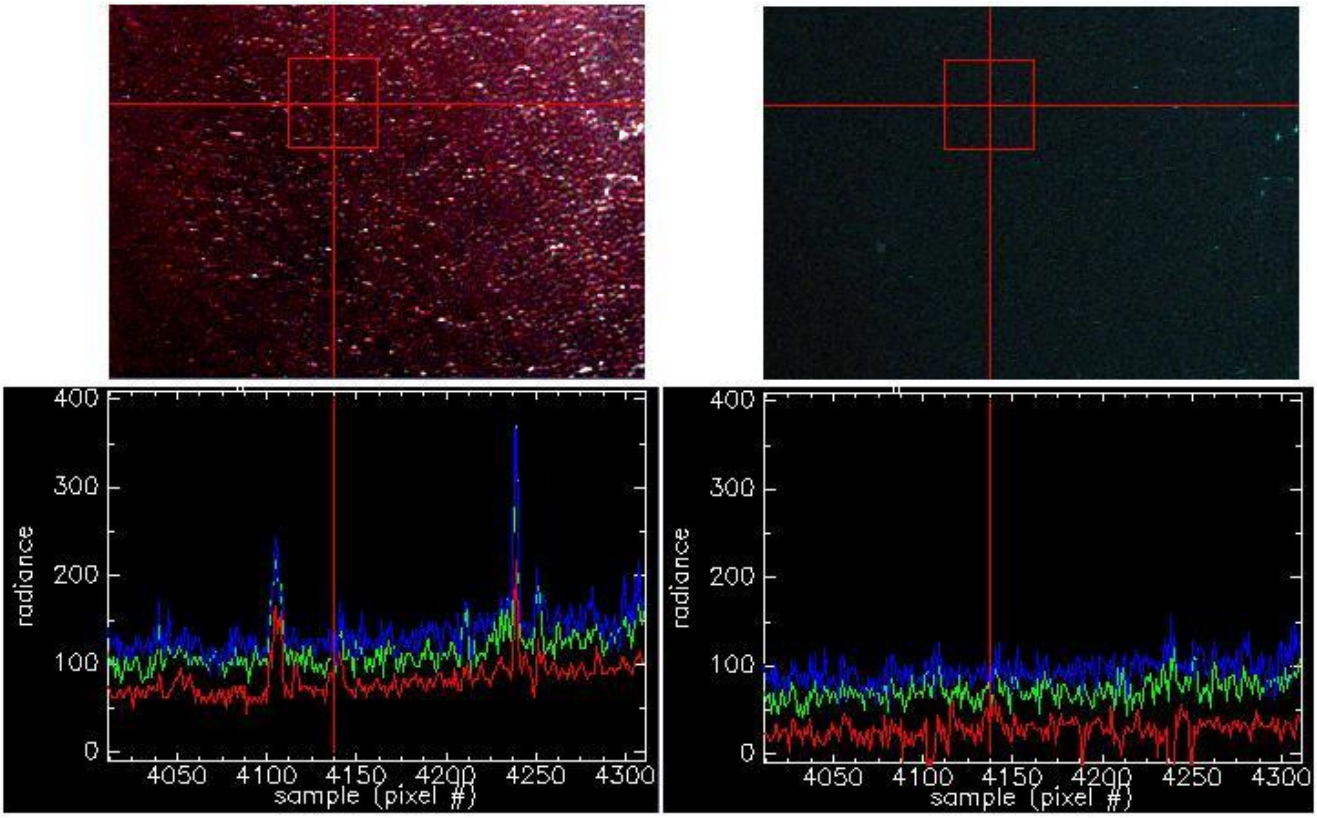


*Figure 7– A sample of the surface glint correction over a portion of deep water in the WorldView-2 image. The correction improved visibility in some areas of the WorldView-2 image by decreasing the "white" signal of whitecaps caused by high reflectance at all wavelengths (a) to yield a smoother looking surface (b). The spectral profile across a portion of the image shows the reflectance peaks of the whitecaps (c) have been removed (d). The blue curve is the blue band 2, green curve is the green band 3, and red curve is the NIR band 8.*

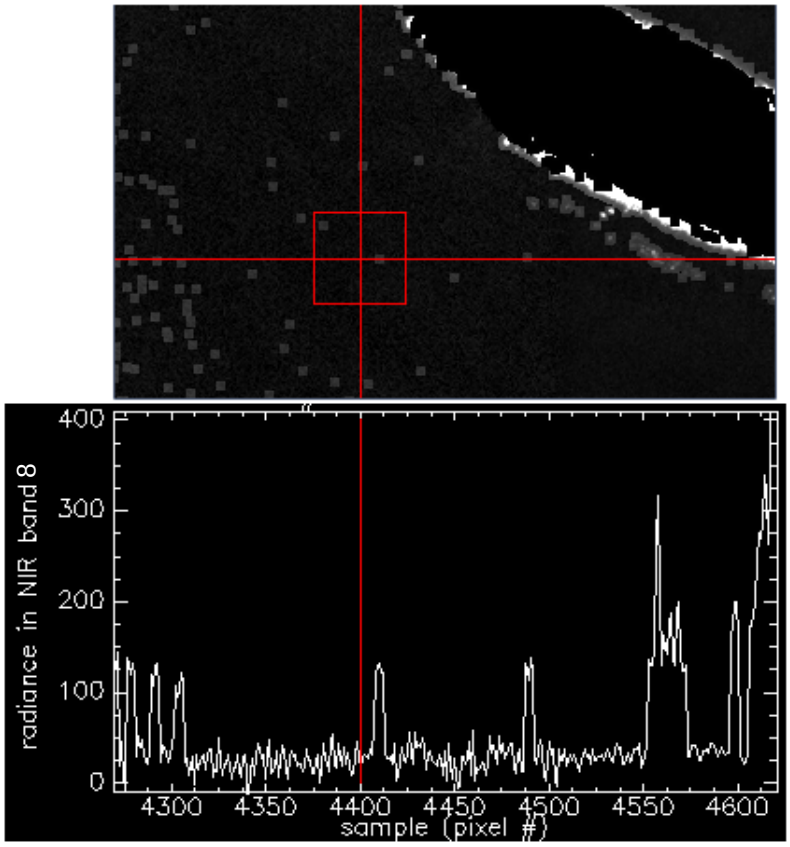


*Figure 8 – A sample of the surface glint correction result on NIR band 8 of the WorldView-2 image, immediately west of Georgeson Island (appears black in the image due to land mask). The correction created high variance for radiance in the NIR band due to the speckled nature of the NIR mask. The NIR mask, designed to keep kelp pixels out of the glint correction to avoid its NIR signal being misidentified as glint and removed, however also kept sporadic high-NIR haze out of the glint correction. This resulted in a glint corrected image with speckled high uncorrected NIR values (seen as lighter grey pixels in the image).*

*Adjacency effect*

The presence of haze and fog in the WorldView-2 image combined with the off-nadir viewing angle of the satellite sensor to create adjacency effects in the water-containing pixels north of the island (Figure 9a-b). This phenomenon is caused by incident light striking vegetation on land and reflecting the vegetation signal at an angle out over the much lower reflectance water. When fog and/or haze are present, the vegetation signal scatters off of the small water droplets in the atmosphere, compounding the signal (Santer and Schmectig, 2000; Sharma et al., 2008). The adjacency effect is characterized in Figure 9c-d, which shows the spectral signature of water pixels moving progressively shoreward. The visible range bands (coastal blue, blue, green, yellow, and red) remain constant while approaching the shoreline, while the near-infrared range bands (705nm and greater; red edge, NIR1, and NIR2) increase exponentially over the same transect. Since NIR bands are the sole bands affected, any band combination between a visible and NIR band is excluded from band selection, as this combination would highlight the adjacency effect. Since the visible range remains unaffected and the NIR bands increase proportionally with one another, band ratios between two visible bands or two NIR bands will not be impacted by the adjacency effect.

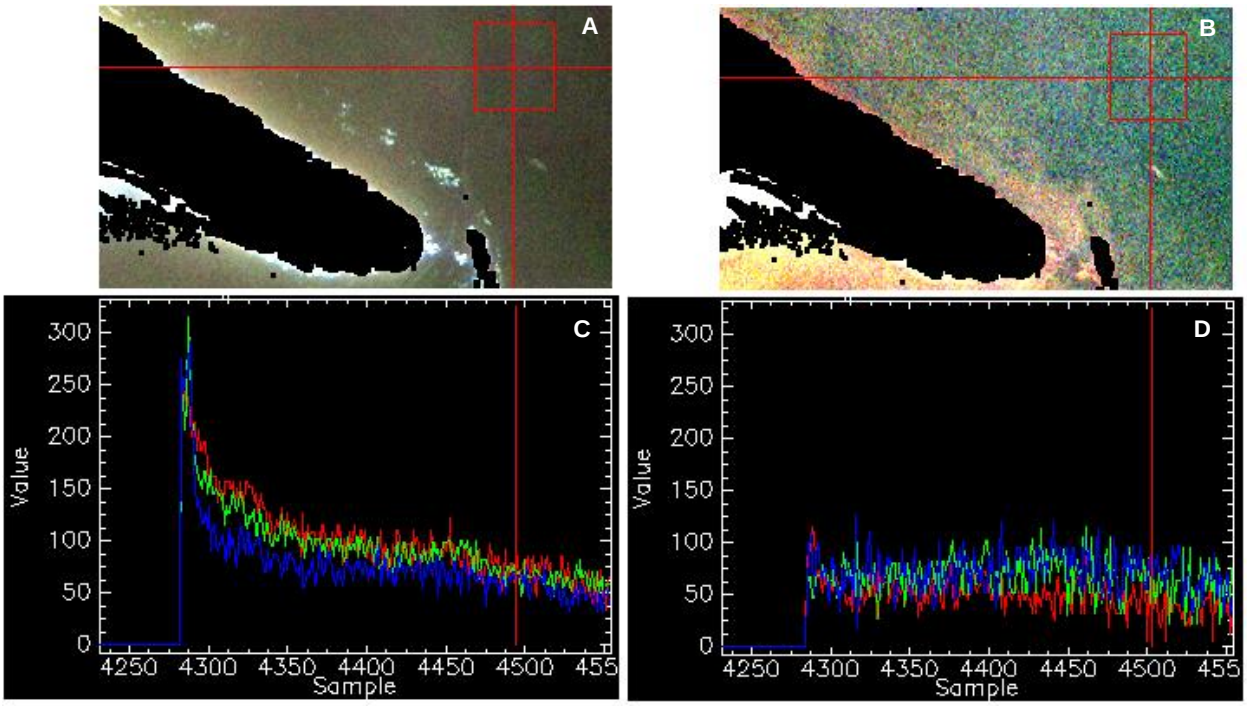


*Figure 9. WorldView-2 false colour image depicting an example of the adjacency effect of land vegetation on neighbouring water pixels as seen in (a) the NIR bands (RGB = band 8, band 7, band 6) and (b) the visible bands (RGB = band 4, band 3, band 2). Incident light strikes vegetation on land and reflecting the vegetation signal at an angle out over the much darker (lower reflectance) water. When fog and/or haze are present, the vegetation signal scatters off of the small water droplets in the atmosphere, compounding the adjacency noise signal. (c) and (d) show the spectral signature of water pixels moving progressively away from shore (land masked as black)in an area of the WorldView-2 image affected by the adjacency effect. Only the near-infrared range bands (bands 6-8) are affected, increasing exponentially toward shore. The visible range bands (bands 1-5) remain constant.*

**B. Image Processing**

*PCA*

The PCA was performed on Worldview-2 bands 1 through 8 for a total of eight PC bands and SPOT6 bands 1 through 4 for a total of four PC bands. For WorldView-2, the first PC band explained 90.3% of the variance, and the loadings showed positive contributions from all eight spectral bands, particularly in the NIR bands, as band 7 contributed 29.9% of the total variance and band 8 contributed 27.3% of the total variance (Table 2 & Figure 10). The majority contribution of the NIR wavelengths to PC1 indicates that this PC band represents, or highlights, features in the image that produce variance in the NIR wavelengths, such as floating kelp, remaining atmospheric effects, white caps, and the land adjacency effect. Similarly, Tables 2 and 3 report the variance explained by each of the WorldView-2 and SPOT-6 PC bands, the percent contribution of the original sensor bands to each PC, and the features of the image that are highlighted by each PC band. Figures 10 and 11 depict graphically the percent contribution of the original sensor bands to each PC. For a depiction of each PC band image to view the features highlighted by each PC band, refer to Appendix A.

*Table 2. Principle component bands (PCs) resulting from principle components analysis of the WorldView-2 image, original band weighting and interpretation of cover classes highlighted by each PC.*

| **WorldView-2** | PC 1 | PC 2 | PC 3 | PC 4 | PC 5 | PC 6 | PC 7 | PC 8 |
|---|---|---|---|---|---|---|---|---|
| % of variance explained | 90.3 | 6.0 | 1.4 | 0.8 | 0.5 | 0.4 | 0.3 | 0.2 |
| Coast Blue (band 1) % contribution | 1.0 | 15.6 | 32.6 | 36.6 | 8.3 | 5.1 | 0.6 | 0.2 |
| Blue (band 2) % contribution | 2.5 | 15.7 | 23.8 | 14.2 | 38.7 | 2.6 | 2.0 | 0.6 |
| Green (band 3) % contribution | 5.6 | 18.4 | 1.3 | 29.1 | 19.1 | 16.0 | 0.1 | 10.4 |
| Yellow (band 4) % contribution | 8.1 | 14.8 | 17.2 | 1.1 | 1.9 | 4.8 | 11.0 | 41.1 |
| Red (band 5) % contribution | 7.3 | 10.8 | 8.4 | 2.9 | 1.7 | 16.9 | 42.5 | 9.5 |
| Red-edge (band 6) % contribution | 18.4 | 0.5 | 5.9 | 14.0 | 13.4 | 6.7 | 21.8 | 19.5 |
| NIR 1 (band 7) % contribution | 29.9 | 11.1 | 0.2 | 0.9 | 2.2 | 20.2 | 18.7 | 16.7 |
| NIR 2 (band 8) % contribution | 27.3 | 13.1 | 10.7 | 1.2 | 14.8 | 27.6 | 3.3 | 2.0 |
| Bands contribute greatest variance | NIR, Re | G,B,CB,Y,R,NIR | CB, B, Y | CB, G, B, Re | NIR, R | NIR, R, G | R, Re, NIR | Y, Re, NIR |
| Interpretation * | variance in NIR highlights floating kelp, adjacency effect | variance in G and R highlights sand. | variance in B and Y highlights sand & green algae | variance in B,G & Re but not NIR highlights submerged kelp | variance in B, Re &NIR highlights floating kelp | equal variance in G, R & NIR highlights white caps | sensor noise | sensor noise |

* visual interpretation of image with local knowledge plus comparison of band variance with spectral fingerprints in Figure 12.

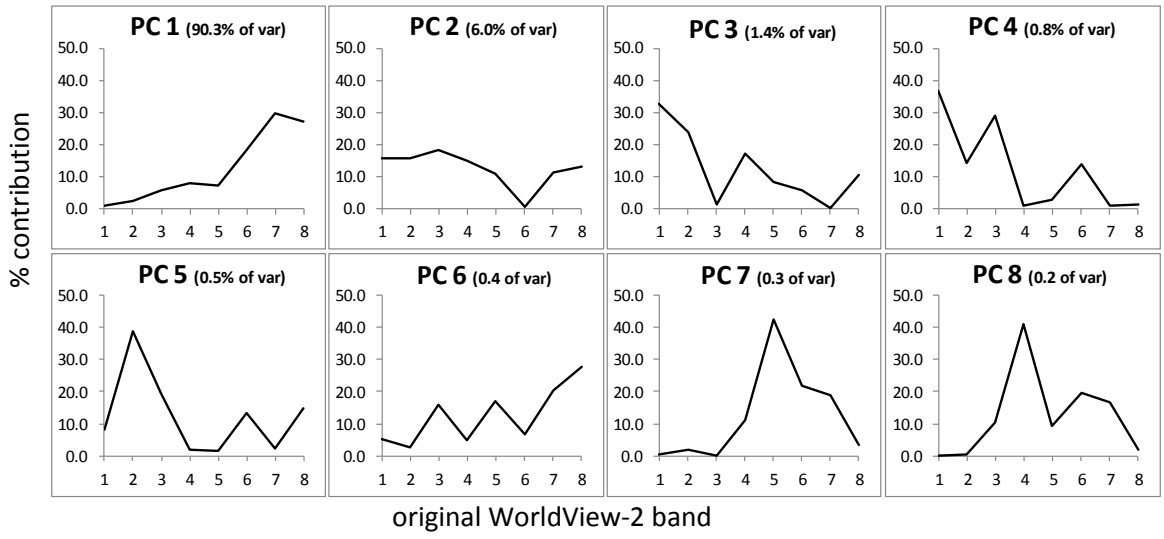


*Figure 10. Band loadings for the principle component bands from PCA of the WorldView-2 image. Each plot represents one PC. On the y-axis is the percent contribution of each original WV-2 band to the PC.*

*Table 3. Principle component bands (PCs) resulting from principle components analysis of the SPOT-6 image, original band weighting and interpretation of cover classes highlighted by each PC.*

| SPOT-6 | PC 1 | PC 2 | PC 3 | PC 4 |
|---|---|---|---|---|
| % of variance explained | 99.47 | 0.50 | 0.03 | 0.01 |
| Blue (band 1) % contribution | 70.8 | 7.0 | 18.2 | 3.9 |
| Green (band 2) % contribution | 22.8 | 1.9 | 29.0 | 46.3 |
| Red (band 3) % contribution | 5.3 | 6.5 | 38.6 | 49.7 |
| NIR (band 4) % contribution | 1.1 | 84.6 | 14.2 | 0.1 |
| Bands contributing greatest variance | B | NIR | R, G, B, NIR | R, G |
| Interpretation | high variance in blue highlights green algae and sand | high variance in NIR highlights floating kelp | medium variance in B, G, R & NIR highlights submerged kelp (flat curve of kelp from B to R) or very shallow green algae/eelgrass with epiphyte | variance in G & R but not B highlights sand |

* visual interpretation of image with local knowledge plus comparison of band variance with spectral fingerprints in Figure 12.

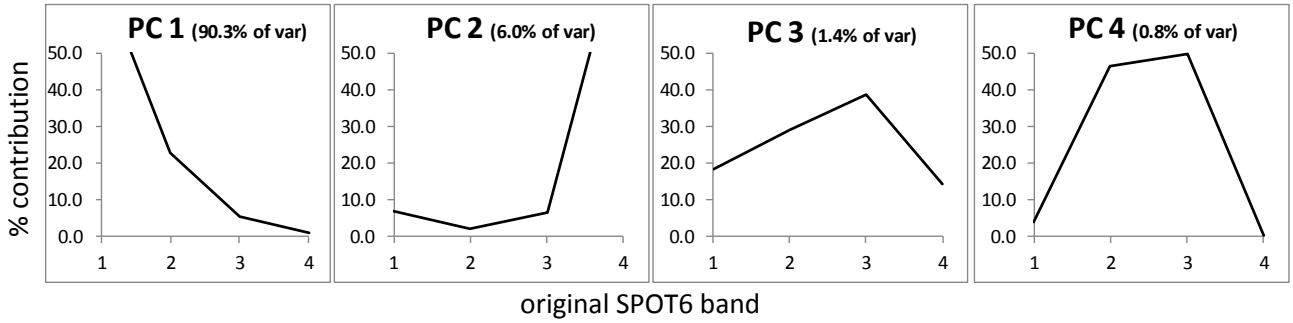


*Figure 11. Band loadings for the principle component bands (PCs) resulting from PCA of the SPOT6 image. Each plot represents one PC. On the y-axis, the band loadings are the percent contribution of each original SPOT band to the specific PC.*

**C. Spectral fingerprints of kelp and associated cover classes**

Spectral fingerprints, or benthic cover spectra, were extracted from a subset of sample pixels throughout the image determined by a combination of ground truth survey data and local knowledge. The spectra are presented in Figure 12a for the WorldView-2 image and Figure 12b for SPOT-6 image. In both cases, kelp has a characteristic NIR signal (WV2 bands 6-8 and SPOT band 4) caused by incident light reflecting off the internal cellular structure of floating bulbs and fronds. There is also a peak in the yellow to red wavelengths

(green to red in the case of SPOT) due to the reflectance peaks of kelp pigment chlorophyll-a (green) and accessory pigment fucoxanthin (yellow/red). The disparity between red and NIR reflectance magnitudes creates a steep slope at the red-edge (WorldView-2 band 6 and SPOT between bands 3 and 4), which varies in magnitude with the degree of submersion of the kelp bed. This phenomenon is due to the variance of NIR reflectance of the kelp with submersion. Pure water is an efficient attenuator of NIR wavelengths, and will absorb all NIR energy within the first few centimetres of the surface. See the deep water curve in Figures 12a and b for an illustration of this NIR absorption.

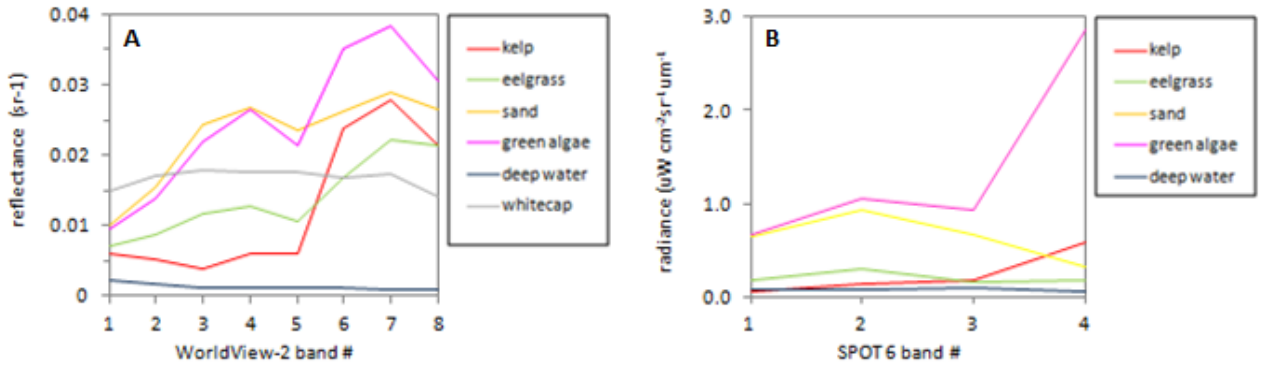


*Figure 12 – Spectral fingerprint of each benthic class in (a) the WV-2 image and (b) the SPOT-6 image. Units are different between the two images due to the differing levels atmospheric correction used (WV-2 in reflectance due to extra haze correction and SPOT-6 in radiance due to single correction for atmosphere), however spectral shape is comparable.*

### *D. Variable set reduction and band selection*

*(i) Band selection: WorldView-2*

***WorldView-2 Case 1**: reflectance bands and reflectance band ratios*

To determine the best bands for separating kelp from the other benthic classes, the M-statistic was employed on the combined set of reflectance bands and reflectance band ratios. For each kelp/other benthic class pair, the M-statistic was calculated at each variable in the initial set of 28 spectral variables. The variable with the greatest M-statistic value (i.e. the variable yielding greatest spectral separation) was identified for each kelp/other substrate pair and are shown together in Table 4. The Case 1 selected variable set included the green band (band 3 i.e., G), NIR-1 (band 7 i.e., N1), and the ratios CB:Y (coastal blue to yellow), Y:Re (yellow to red edge), and R:N1 (red to NIR1). The separability of the benthic classes provided by these five spectral variables is shown in Figure 13, as produced by the ENVI 'n-d visualizer' application.

*Table 4. Case 1 selected variable set resulting from M-statistic analysis of the WorldView-2 reflectance bands and band ratios. The greatest M-statistic value for each kelp-substrate pair is identified with a black box. Refer to Appendix C to view the M-statistic results for the full list of WorldView-2 bands, band ratios, and PC bands. Refer to Appendix E for the band images of the selected variables.*

| | M-statistic between kelp and: | | | | |
|---|---|---|---|---|---|
| spectral variable | sand | eelgrass | green algae | deep water | whitecap |
| G | 0.8 | 1.3 | **1.9** | 0.8 | 0.7 |
| N1 | 0.2 | 0.5 | 0.0 | **2.9** | 0.8 |
| CB:Y | **1.2** | 0.5 | 1.1 | 0.1 | 0.1 |
| Y:RE | 0.8 | **2.1** | 1.6 | 0.3 | 2.0 |
| R:N1 | 0.8 | 1.6 | 1.4 | 0.3 | **2.3** |

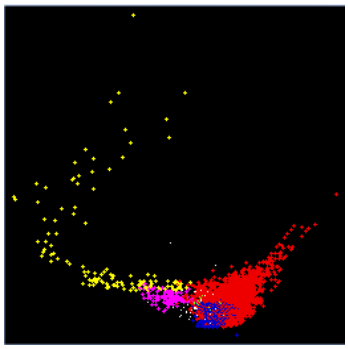

*Figure 13. Separability between kelp (red) and all other benthic classes offered by the Case 1 selected variable set, represented in 2D space (G, N1, CB:Y, Y:Re, and R:N1). Red = kelp, Yellow= sand, green = eelgrass, magenta = green algae, blue = deep water.*

***WorldView-2 Case 2**: PC Analysis bands*

In Case 2, the M-statistic analysis was employed on the set of PC bands resulting from the principle components analysis of the WorldView-2 image. Again, for each kelp/other benthic class pair, the M-statistic was calculated at each variable in the initial set of eight spectral variables. The variable with the greatest M-statistic value (i.e. the variable yielding greatest spectral separation) was identified for each kelp/other substrate pair and are shown together in Table 5. The Case 2 selected variable set included PC1, PC3, PC4, PC5 and PC6. The separability of the benthic classes provided by these five spectral variables is shown in Figure 14. Via progressive trials of variable removal in the ENVI n-d visualizer, it was determined that the best spectral separation resulted from a further removal of PC3 and PC6, for a final Case 2 selected variable set of PC1, PC4, and PC5.

*Table 5. Case 2 selected variable set resulting from M-statistic analysis of the WorldView-2 principle component bands. The greatest M-statistic value for each kelp-substrate pair is identified with a black box. Refer to Appendix C to view the M-statistic results for the full list of WorldView-2 bands, band ratios, and PC bands. Refer to Appendix E for the band images of the selected variables.*

| | M-statistic between kelp and: | | | | |
|---|---|---|---|---|---|
| spectral variable | sand | eelgrass | green algae | deep water | whitecap |
| PC1 | 0.6 | 0.3 | 0.5 | **2.8** | 0.2 |
| PC3 | 1.7 | 0.3 | **1.3** | 0.2 | 0.0 |
| PC4 | **2.6** | 1.7 | 0.6 | 1.8 | 1.0 |
| PC5 | 1.4 | **1.8** | 0.4 | 1.9 | 0.9 |
| PC6 | 1.5 | 1.5 | 0.2 | 1.9 | **1.4** |

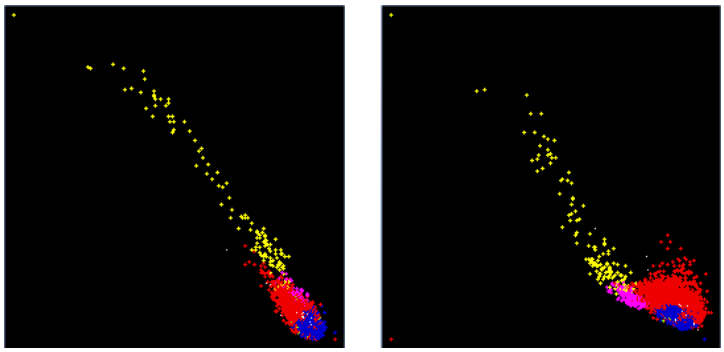

*Figure 14. Separability between kelp (red) and all other benthic classes offered by the Case 2 selected variable set represented in 2D space (a) after M-statistic selection (PC1,4,5 and 6) and (b) after secondary removal of variables PC1 and PC6 via ENVI n-d visualizer (PC1,4 and 5). Red = kelp, yellow= sand, green = eelgrass, magenta = green algae, blue = deep water.*

*(ii) Band selection: SPOT-6*

***SPOT Case 1**: reflectance bands and reflectance band ratios*

As in WorldView-2, above, the M-statistic was employed on the combined set of SPOT-6 reflectance bands and reflectance band ratios. For each kelp/other benthic class pair, the M-statistic was calculated at each variable in the initial set of ten spectral variables. The variable with the greatest M-statistic value (i.e. the variable yielding greatest spectral separation) was identified for each kelp/other substrate pair and all are shown together in Table 6. The Case 1 selected variable set included the red band (band 3), and ratios B:R and G:NIR. The separability of the benthic classes provided by these three spectral variables is shown in Figure 15.

*Table 6. Case 1 selected variable set resulting from M-statistic analysis of the SPOT-6 reflectance bands and band ratios. The greatest M-statistic value for each kelp-substrate pair is identified with a black box. Refer to Appendix D to view the M-statistic results for the full list of WorldView-2 bands, band ratios, and PC bands. Refer to Appendix F for the band images of the selected variables.*

| spectral variable | M-statistic between kelp and: | | | |
|---|---|---|---|---|
| | **sand** | **eelgrass** | **green algae** | **deep water** |
| R | 1.4 | 0.2 | 11.2 | 1.1 |
| B:R | 2.1 | 1.9 | 1.6 | 1.7 |
| G:NIR | 2.7 | 1.1 | 0.7 | 5.2 |

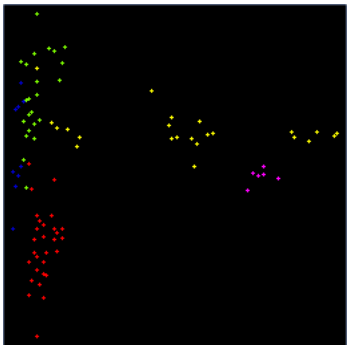

*Figure 15. Separability between kelp (red) and all other benthic classes offered by the Case 1 selected variable set of SPOT-6 (R, B:R, and G:NIR) represented in 2D space. Red = kelp, yellow= sand, green = eelgrass, magenta = green algae, blue = deep water.*

***SPOT Case 2**: PC Analysis bands*

In Case 2, the M-statistic analysis was employed on the set of PC bands resulting from the principle components analysis of the SPOT-6 image. The variable with the greatest M-statistic value (i.e. the variable yielding greatest spectral separation) was identified for each kelp/other substrate pair and are shown together in Table 7. The Case 2 selected variable set included PC1, PC2 and PC3. Via progressive trials of variable removal in the ENVI n-d visualizer, it was determined that the best spectral separation resulted from a further removal of PC1, for a final Case 2 selected variable set of PC2 and PC3. The separability of the benthic classes provided by these two spectral variables is shown in Figure 16.

*Table 7. Case 2 selected variable set resulting from M-statistic analysis of the SPOT-6 principle component bands. The greatest M-statistic value for each kelp-substrate pair is identified with a black box. Refer to Appendix D to view the M--statistic results for the full list of WorldView-2 bands, band ratios, and PC bands. Refer to Appendix F for the band images of the selected variables.*

| spectral variable | M-statisic between kelp and: | | | |
|---|---|---|---|---|
| | **sand** | **eelgrass** | **green algae** | **deep water** |
| PC1 | 1.7 | 0.7 | 9.5 | 0.7 |
| PC2 | 0.5 | 1.8 | 7.9 | 2.3 |
| PC3 | 1.9 | 1.2 | 1.2 | 1.5 |

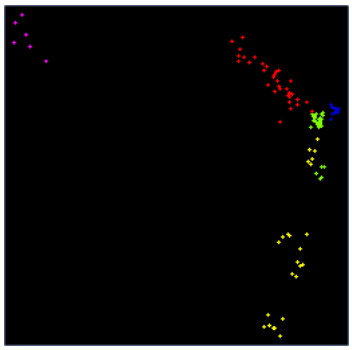

*Figure 16. Separability between kelp (red) and all other benthic classes offered by the Case 2 selected variable set of SPOT-6 (PC2 and PC3) represented in 2D space. Red = kelp, yellow= sand, green = eelgrass, magenta = green algae, blue = deep water.*

Since the variable selection process selects variables for which the spectral separation between kelp and other benthic cover classes is the greatest, the kelp spectral features present at these variables are therefore the most unique to the kelp class. The unique kelp features being recognized by the selected variables of both sensors are the NIR peak of floating kelp, the red-edge peak of submerged kelp, and kelp's small amplitude and flat slope through the green to red range relative to other benthic classes (for example, the medium amplitude green peak of green algae and eelgrass and the high amplitude red peak of sand). In the case of WorldView-2, kelp displayed a slight negative slope between the blue and green wavelengths, which caused additional selection of variables relating to the blue range (refer to Figures 10 and 12, previously).

**E. Classification and Validation**

The results of classification of the WorldView-2 image via maximum likelihood classifier are shown in Figure 17. Producer accuracies are reported in Table 8 and each map is depicted as an overlay over the ground truth survey distribution in Figure 18 for an additional visual validation of areal distribution. The results of kelp classification of the SPOT-6 image via maximum likelihood classifier are shown in Figure 19. Producer accuracies are reported in Table 8 and each satellite kelp map is depicted as an overlay over the ground truth kelp survey distribution polygons in Figure 20 for an additional visual validation of areal distribution match. The visual comparison between ground data maps and satellite image classifications are made by assessing the kelp map for a match to the ground truth kelp survey map in terms of general location, shape, area, and environmental context. For example a linear kelp bed which is the same size and length as the kelp ground truth survey map, but skewed four metres to the west would be considered a good match even though not directly overlapping due to the context of tidal drift over time.

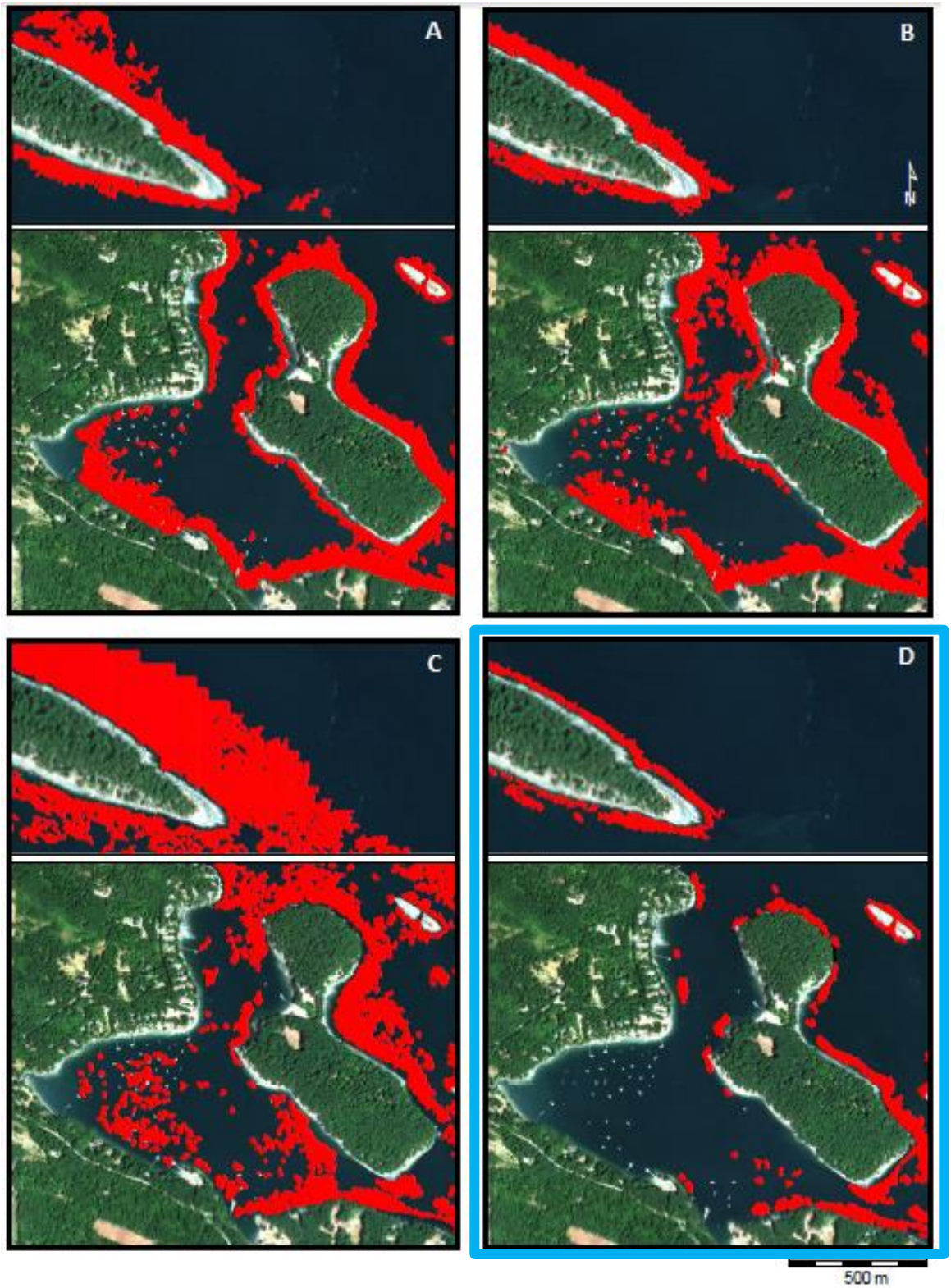


*Figure 17. Classification results for the WorldView-2 image. Kelp distribution for each selected variable set is shown in red overlain on the true colour WorldView-2 image. Classifications are of the (a) WorldView-2 reflectance image with no variable selection: bands 1 - 8; (b) WorldView-2 image of most effective kelp bands selected from all reflectance bands and reflectance band ratios (Case 1): G, N1, CB:Y, Y:Re, and R:N1; (c) WorldView-2 PCA image with no variable selection: PC 1-8;* ***(d) WorldView-2 image of most effective kelp bands selected from all PC bands (Case 2): PC1, PC4 and PC5 (produced the best results).*** *For each instance, the upper and lower figures are MICS Kelp Survey Area 6 around Georgeson Island and MICS Kelp Survey Area 9 around Curlew Island, respectively.*

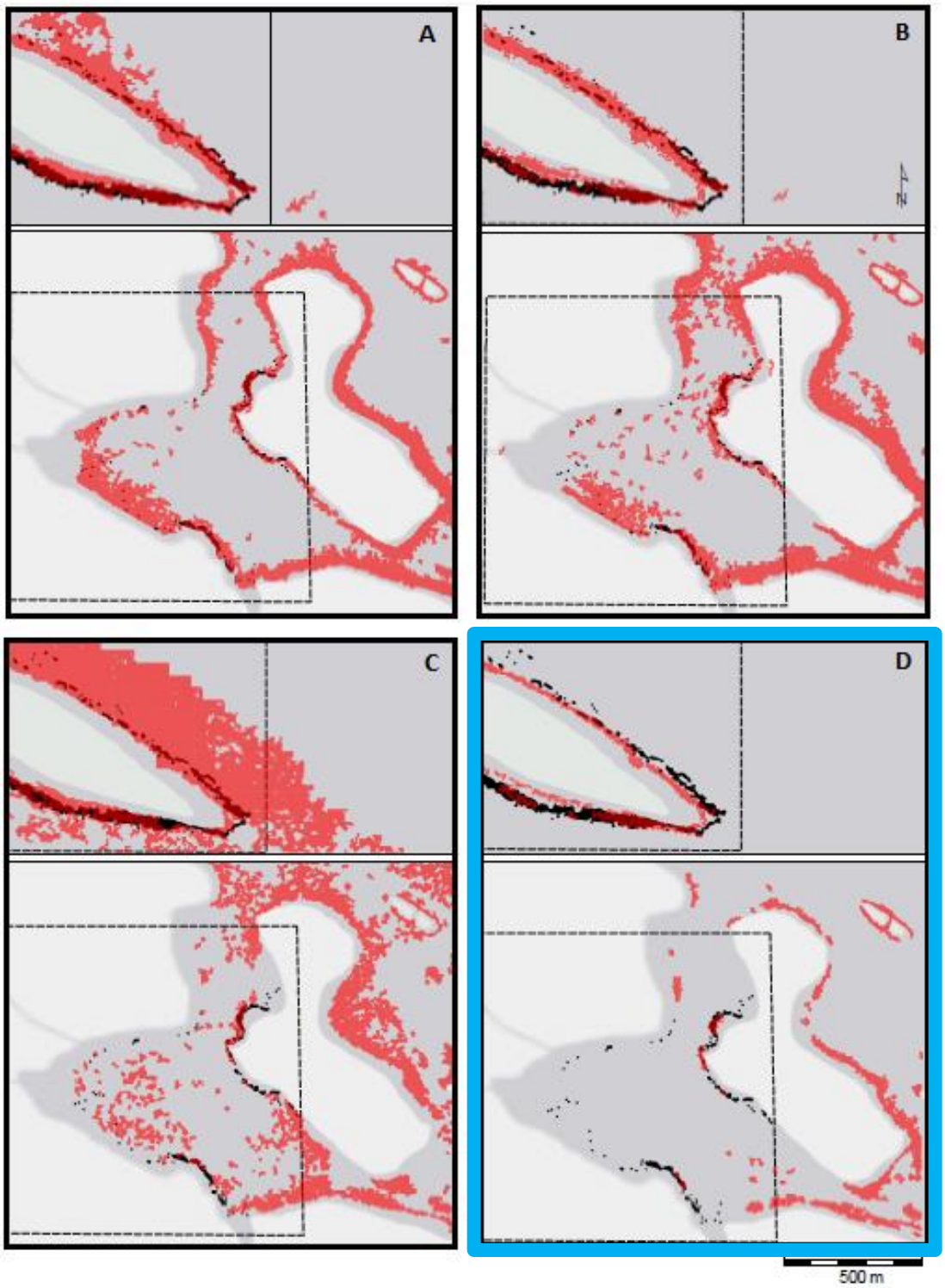


*Figure 18. WorldView-2 kelp classification results overlain on the 2013 MICS kelp ground truth survey data for visual comparison of the spatial accuracy of each product. The area covered by ground truth survey is outlined by the black dashed line and denotes the validation region. Ground truth survey kelp distribution is shown in black, while satellite derived kelp distribution are in red transparency. (a) Classification before band selection – bands CB, B, G, Y, R, Re, N1, N2; (b) Classification after band selection – bands G, N1, CB:Y, Y:Re, R:N1 (red to NIR1) (c) Classification PCA image before band selection- PC bands 1-8;* ***(d) Classification PCA image after band selection – PC bands 1, 4 & 5 (produced the best results).*** *For each instance, the upper and lower figures are MICS Kelp Survey Area 6 around Georgeson Island and MICS Kelp Survey Area 9 around Curlew Island, respectively.*

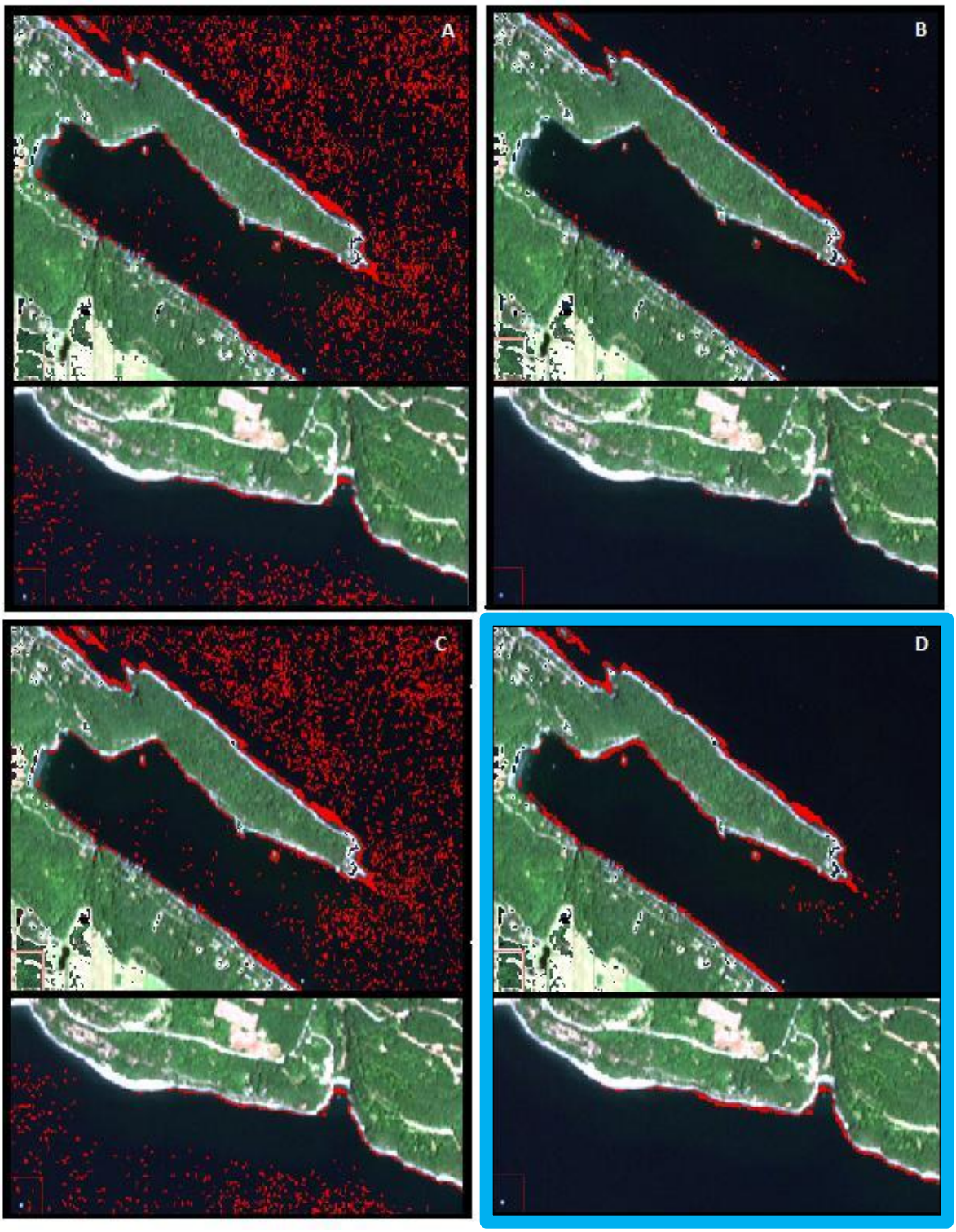


*Figure 19. Classification results for the SPOT-6 image. Kelp distribution for each selected variable set is shown in red over the true colour SPOT-6 image. (a) SPOT-6 reflectance image with no variable selection: bands 1 - 4; (b) SPOT-6 image of most effective kelp bands selected from all reflectance bands and reflectance band ratios (Case 1): R, B:R and G:NIR; (c) SPOT-6 PCA image with no variable selection: PC 1-4; (**d) SPOT-6 image of most effective kelp bands selected from all PC bands (Case 2): PC2 and PC3 (produced the best results)**. For each instance, the locations are MICS Kelp Survey Areas 3, 4 and 5 around Edith Point and the north portion of Campbell Bay (upper) and MICS Kelp Survey Area 11 along a portion of Navy Channel (lower).*

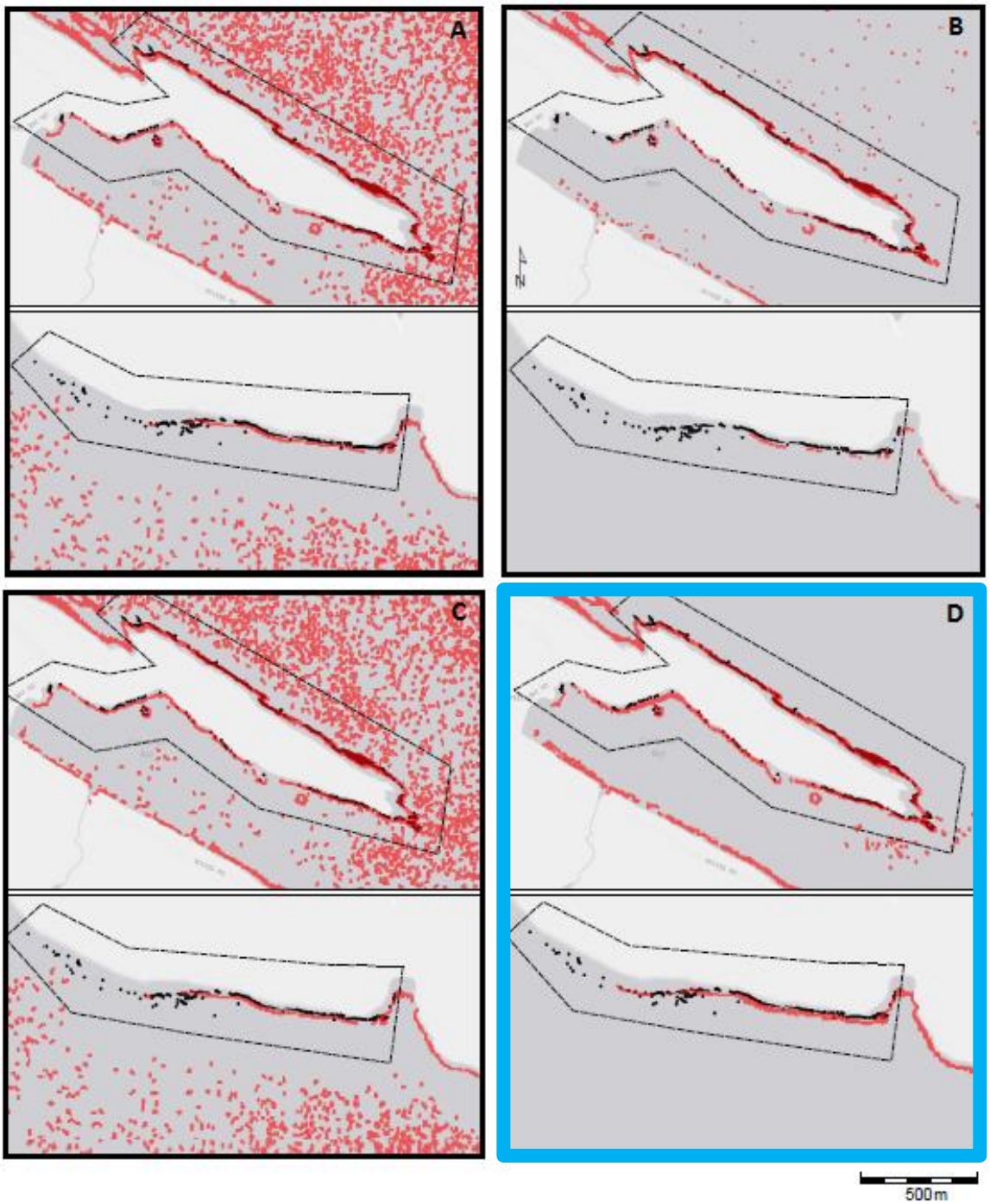


*Figure 20. SPOT-6 kelp classification results overlain on the 2014 MICS kelp ground truth survey data for visual comparison of the spatial accuracy of each product. The area covered by ground truth survey is outlined by the black dashed line and denotes the validation region. Ground truth survey kelp distribution is shown in black, while satellite derived kelp distribution are in red transparency. (a) Classification before band selection – bands B, G, R, NIR; (b) Classification after band selection – bands R, B:R, G:NIR; (c)Classification PCA image before band selection- PC bands 1-4;* ***(d) Classification PCA image after band selection – PC bands 2 & 3 (produced the best results).*** *For each instance, the locations are MICS Kelp Survey Areas 3, 4 and 5 around Edith Point and the north portion of Campbell Bay (upper) and MICS Kelp Survey Area 11 along a portion of Navy Channel (lower).*

*Table 8. Producer and user accuracies for each WorldView-2 and SPOT-6 kelp classification scenario.*

| Sensor | Bands | Area | accuracy | visual distribution rank |
|---|---|---|---|---|
| WV-2 | CB, B, G, Y, R, Re, N1, N2 | Georgeson, Curlew | 78.13 | 3 |
| WV-2 | G, NIR, CB:Y, Y:Re, R:N1 | Georgeson, Curlew | 60.74 | 2 |
| WV-2 | Full PCA (PC1-PC8) | Georgeson, Curlew | 65.38 | 4 |
| **WV-2** | **PC1, PC4, PC5** | **Georgeson, Curlew** | **30.06** | **1** |

| Sensor | Bands | Area | accuracy | visual distribution rank |
|---|---|---|---|---|
| SPOT6 | B, G, R, NIR | Edith, Navy | 61.27 | *3* |
| SPOT6 | R, B:R, G:NIR | Edith, Navy | 52.68 | *2* |
| SPOT6 | Full PCA (PC1-PC4) | Edith, Navy | 61.27 | *3* |
| **SPOT6** | **PC2, PC3** | **Edith, Navy** | **61.60** | ***1*** |

The best kelp map product was produced from the SPOT-6 image, with the selected variable set of principle component (PC) bands 2 and 3 *(Figure 19d & 20d)*. The SPOT-6 PC2, PC3 kelp map had a producer accuracy of 61.6%, however, ***the statistic is an assumed underestimate of the true accuracy due to (1) the mobility of kelp beds at the surface with changing water depth and current direction throughout tidal cycles and (2) the fast growth rate of Nereocystis rapidly changing the standing crop of kelp between the time of image acquisition and the time of kelp survey***. Figure 20 illustrates the slight drift of linear beds of kelp, notably within the inner (northern) reaches of Campbell Bay and the east end of the Navy Channel subset.

F. Panchromatic Sharpening

Gram-Schmidt panchromatic sharpening transformation was performed on the SPOT-6 PC2, PC3 variable set to test for improvement in kelp mapping accuracy with increased spatial resolution. The SPOT-6 panchromatic image was merged with each of the SPOT-6 PC2 and PC3 bands to increase their resolution (pixel size) from 6m to 1.5m (Figure21 a and b respectively). Maximum likelihood classification was run once more on the higher resolution set. The results are shown in Figure 21. The resulting kelp distribution had greater detail along the polygon edges at 1.5m than at 6m resolution and remains a good visual match to the ground truth kelp distribution (Figure 21c-d). However, due to the low signal to noise ratio of the panchromatic band, some noise is introduced into the kelp map in the form of small false kelp patches in the deep water area to the north of Edith Point (Figure 21b & d) and classification accuracy decreased to 40.1%.

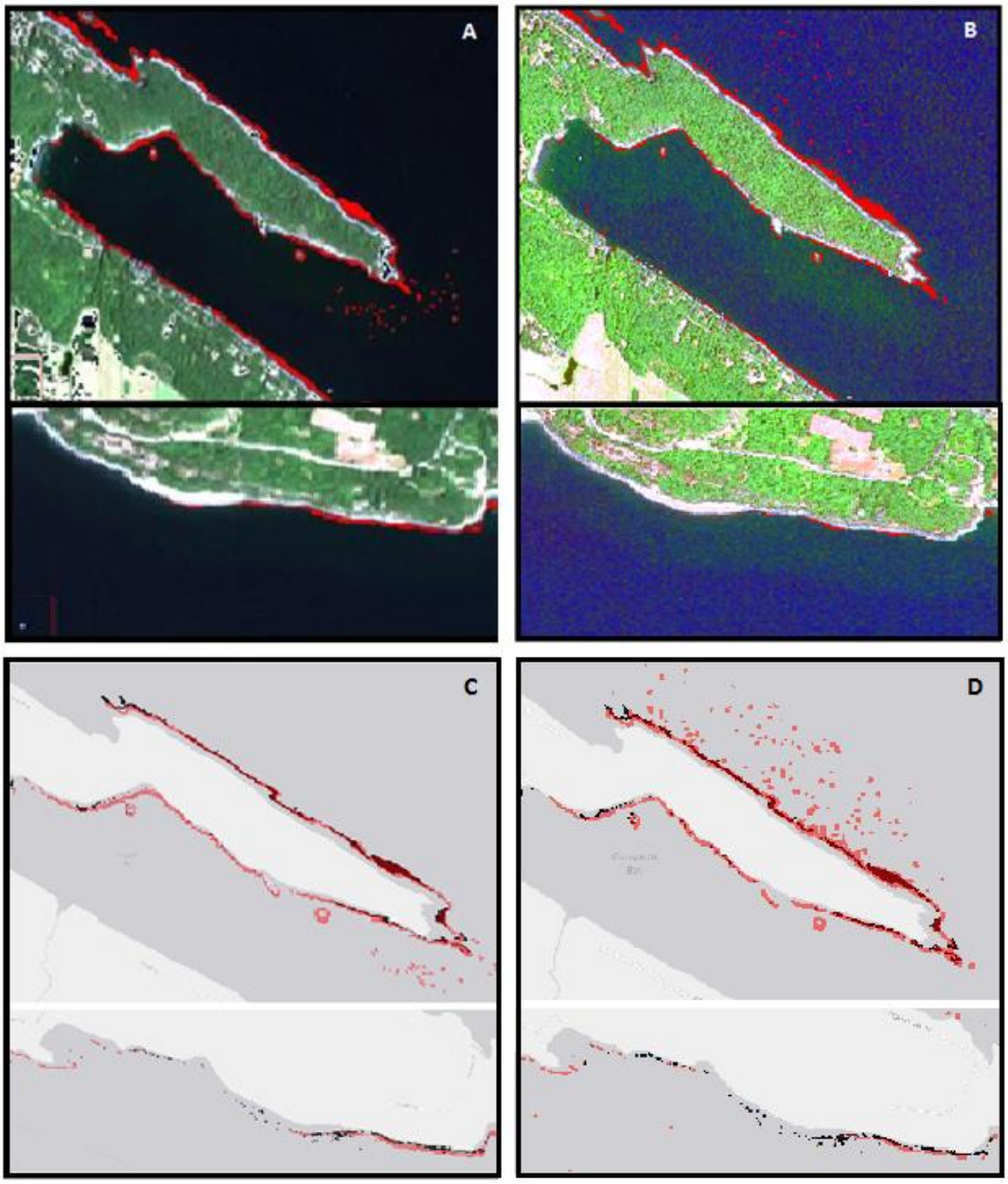


*Figure 21. Classification results for the spectral variable set offering best kelp mapping results (SPOT-6 PC2 & PC3) (a) before and (b) after Gram-Schmidt pan-sharpening transformation to increase spatial resolution. Areas shown are Edith Point (upper) and Navy Channel (lower). Notice the improvement in spatial detail in the pan-sharpened image (b). The kelp classification is shown in red, while the ground truth survey kelp distribution is shown in black (c,d).*

## V. Conclusions

The current pilot study demonstrated the use of satellite optical imagery to map the canopy distribution of kelp *Nereocystis leutkeana.* While pre-processed, but mathematically unaltered imagery consisting of radiance/reflectance spectral variables was able to detect kelp canopies, ***a pre-processed and reduced set of spectral variables (band ratios and PCA bands) offered a more accurate kelp map*** product with lesser interference from atmospheric, sea surface, and sensor noise effects, and less confusion with other benthic cover classes. Both sensors were shown to be capable of delineating kelp canopies: WorldView-2 with its 8 spectral bands and higher resolution (2m), and SPOT-6 with its 4 spectral bands and lower spatial resolution

(6m). In the case of WorldView-2, the best spectral variables for maximizing spectral separation between kelp and other benthic cover classes were G, NIR, CB:Y, Y:Re, R:N1 or principle component PC1, PC4 and PC5 which emphasize variance in the NIR, red-edge and green and blue wavelength ranges, variously. In the case of SPOT-6, the most important spectral variables for mapping kelp were B:R, G:NIR, or principle component PC2 and PC3, which emphasize variance in the NIR and green to red ranges, respectively.

Since the variable selection process selects variables for which the spectral separation between kelp and other benthic cover classes is greatest, the kelp spectral features present at these variables are therefore the most unique to the kelp class. The kelp features recognized by the selected spectral variables of both sensors are the NIR peak of floating kelp, the red-edge peak of submerged kelp, and kelp's small amplitude and flat slope through the green to red range relative to other benthic classes (for example, the medium amplitude green peak of green algae and eelgrass and the high amplitude red peak of sand). In the case of WorldView-2, kelp displays a slight negative slope between the blue and green wavelengths, which caused additional selection of variables relating to the blue range.

The best kelp map product attained in this study was produced from the SPOT-6 image, with the selected variable set of principle component PC2 and PC3 after image preprocessing steps of georectification, atmospheric correction, masking of land and depth below 30 m, and the statistical image processing steps of principle components analysis (PCA) and variable reduction (Figure 22). The kelp map product had a producer accuracy of 61.6%, however, the statistic is an assumed underestimate of the true accuracy due to (1) the mobility of kelp beds at the surface with changing water depth and current direction throughout tidal cycles; (2) the fast growth rate of *Nereocystis* rapidly changing the standing crop of kelp between the time of image acquisition and the time of kelp survey. Figures 20 a-d and Figure 22 insets illustrate the slight drift of linear beds of kelp, notably within the inner (northern) reaches of Campbell Bay and the east end of the Navy Channel subset. (3) Locational error intrinsic in field surveys due to occasional human error, the accuracy level of the GPS, and availability of satellites to the GPS unit; Some areas of the kelp survey had lower accuracies due to forest cover and rock formations near the shoreline (MICS, 2015b).

Applying panchromatic sharpening transformation produced a kelp map with greater detail along polygon edges due to its finer spatial resolution. However, since the panchromatic band characteristically has a low signal to noise ratio over water (i.e. high noise), some noise was introduced into the kelp map in the form of error over deep water areas, where small false kelp patches appeared.

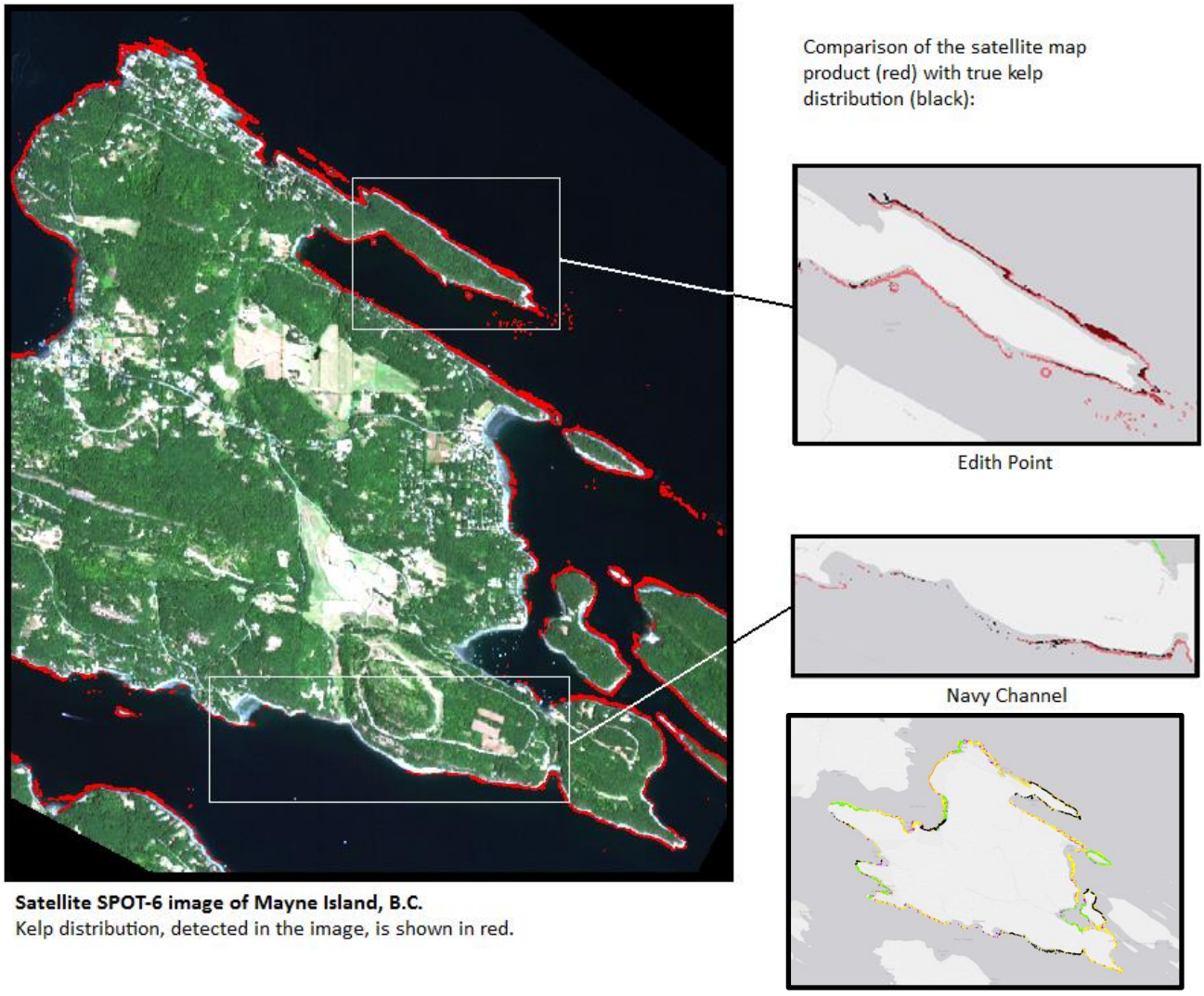


*Figure 22. Best kelp classification yielded by the current study was produced from the SPOT-6 satellite image with the preprocessing steps of georectification, atmospheric correction, land and 30m depth mask and statistic image processing stages of principle components analysis and variable selection. Variables used in classification were principle component PC2 and PC3. Lower right figure is a compilation of kelp mapping data from 2010-2014 for Mayne Island. Note that there was no* in situ *kelp data for validation of the entire Mayne Island 2014 kelp product. Additional field data would be required for full validation of this product.*

The coverage of the derived kelp map product is dependent on the availability of cloud-free, low tide imagery, acquired during peak kelp growth months of August through September. The accuracy of the kelp map product is dependent on (1) atmospheric conditions, (2) sea surface conditions, (3) the acquisition angle of the sensor, and (4) noise introduced by the optical sensor itself. The most notable atmospheric conditions are fog and haze, which, as demonstrated with the WorldView-2 image in the present study, interfere with detection of the NIR signal of floating kelp canopies by adding false NIR reflectance levels. Fog and haze also create and amplify an adjacency effect or “shadow” effect over benthic pixels, whereby at high sensor acquisition angles, the high amplitude signal of land vegetation is transferred to benthic pixels immediately adjacent on the leeward side. It is for these reasons that the authors recommend the following criteria for satellite optical imagery acquisition for the purpose of kelp canopy mapping:

- Cloud free (maximizes mappable area)
- Minimal haze and fog coverage (maximizes mappable area and minimizes adjacency effect)
- Sensor acquisition angle close to nadir (maximizes signal, minimizes atmospheric interference and adjacency effect)
- Low tide level (maximizes the amount of kelp canopy that reaches the surface and therefore to the sensor)
- Acquired during the peak kelp growth months of August through September

Furthermore, for the greatest kelp mapping accuracy, it is recommended that the following imaging processing methodologies are carried out on the acquired imagery:

- Georectification
- Atmospheric correction
- Haze correction (if haze is present)
- Land mask
- Cloud mask (if clouds are present)
- 30 metre depth mask
- Principle Components Analysis
- Variable Selection

**VI. Future Direction & Cost Estimate**

The remote kelp mapping method explored in this pilot project may be applied to the complete area of the Salish Sea to obtain a current distribution map of kelp in the area. Given the approximate coastal surface area of the Salish Sea between Desolation Sound and Puget Sound is approximately 25,000 $km^2$, the cost of imagery would be approximately $50,000 – $60,000 (this is with a research discount for UVic) for a complete set of SPOT-6/7 images. The project would be of a scope and duration as determined by the needs of the Pacific Salmon Foundation and its affiliated stakeholders during consultation and is dependent on the availability of qualified personnel in the SPECTRAL lab at UVic at the time of call for proposals.

**VIII. REFERENCES**


Byrnes, J., Reed, D., Cardinale, B., Cavanaugh, K., Holbrook, S., Schmitt, R. (2011). Climate driven increases in storm frequency simplify kelp forest food webs. Glob Change Biol, 17(8): 2513-2524

Cavanaugh, K., Siegel, D., Kinlan, B., Reed, D. (2010). Scaling giant kelp field measurements to regional scales using satellite observations. Mar. Ecol. Prog. Ser. 403:13-27.

Cavanaugh, K., Siegel, D., Reed, D., Dennison, P. (2011). Climate controls on the giant kelp populations of the Santa Barbara Channel, California. Mar. Ecol. Prog. Ser. 429: 1-17.

Guild, L., Cohen, W., Kauffman, J. (2004). Detection of deforestation and land conversion in Rondoˆnia, Brazil using change detection techniques. *Int. J. Remote Sensing, 25 (4): 731–750.*

Hedley, J., Harborne, A., Mumby, P. (2005). Simple and robust removal of sun glint for mapping shallow-water benthos. Int J Remote Sens. 26: 2107-2112.

Help the Kelp. (2015). Help the Kelp Citizen Science Project – Gabriola Island. *Accessed via the World Wide Web at: http://helpthekelp.blogspot.ie/*

Jensen, J. (1996).Introductory digital image processing. Ed. Clarke, K., Prentice Hall, New Jersey.

Jiang, C., Zhao, H., Jia, G. (2012). Estimation of adjacency effect in the remotely sensed Hyperspectral data over rugged scenes. *IEEE International Conference on Imaging Systems and Techniques (IST), 2012*

Kirk, J. (1994). Light & Photosynthesis in Aquatic Ecosystems, University Press, Cambridge.

Macleod, R. D., & Congalton, R G. (1998). Quantitative comparison of change detection algorithms for monitoring eelgrass from remotely sensed data. *Photogrammetric Engineering and Remote Sensing*, *64*(3), 207-216.

Maritorena, S., Morel, A., Gentili, B. (1994). Diffise reflectance of oceanic shallow waters: Influence of water depth and bottom albedo. Limnol Oceanogr. 39(7): 1689-1703.

Mayne Island Conservation Society. (2010). Guidelines and methods for mapping and monitoring kelp forest habitat in British Columbia. Prepared for the Seagrass Conservation Working Group.

Mayne Island Conservation Society. (2015a, unpublished). Monitoring plan for Mayne Island bull kelp.

Mayne Island Conservation Society. (2015b, unpublished). Kelp Habitat Mapping – Mayne Island, BC. Metadata.

Montes, Marcos, Gao, B., Davis, Curtiss O. (2004). NRL Atmospheric Correction Algorithms for Oceans : Tafkaa User's Guide. Distribution. 1-39.

O'Neill, J. & Costa, M. (2013). Mapping eelgrass (Zostera marina) in the Gulf Islands National Park Reserve of Canada using high spatial resolution satellite and airborne imagery. Remote Sens Environ. 133: 152–167.

O'Neill, J., Costa, M., Sharma, T., (2011). Remote sensing of shallow coastal benthic substrates: in situ spectra and mapping of eelgrass (Zostera marina) in the Gulf Islands National Park Reserve of Canada. Remote Sens. Special issue: Remote Sensing in Coastal Ecosystems, 3 (5), 975-1005.

Reshitnyk, L., Costa, M., Robinson, C., Dearden, P. (2014). Evaluation of WorldView-2 and acoustic remote sensing for mapping benthic habitats in temperate coastal Pacific waters. Remote Sens Environ. 153: 7-23.

Richards, J.A. (1999). Remote Sensing Digital Image Analysis, *Springer-Verlag, Berlin, p. 240.*

Santer, R., and C. Schmechtig (2000). Adjacency effect on water surfaces: primary scattering approximation and sensitivity study. Appl. Opt., 39, 361-375.

Sharma, A., Badarinath, K., Roy, P. (2008). Corrections for atmospheric and adjaceny effects on high resolution sensor data – a case study using IRS-P6 LISS-IV data. *The International Archives of the Photogrammetry, Remote Sensing and Spatial Information Sciences, 37(8), Beijing 2008.*

Springer, Y., Hays, C., Carr, M., Mackey, M. (2007). Ecology and management of the bull kelp, *Nereocystis luetkeana*: A Synthesis with Recommendations for Future Research. A report initiated and supported by the Lenfest Ocean Program

Story, M., & Congalton, Russell G. (1986). Accuracy Assessment : A User ' s Perspective. *Photogrammetric Engineering and Remote Sensing*, 52(3), 397-399.

**Appendix A – Band images for each PC band resulting from principle components analysis (PCA) of the WorldView-2 image.**

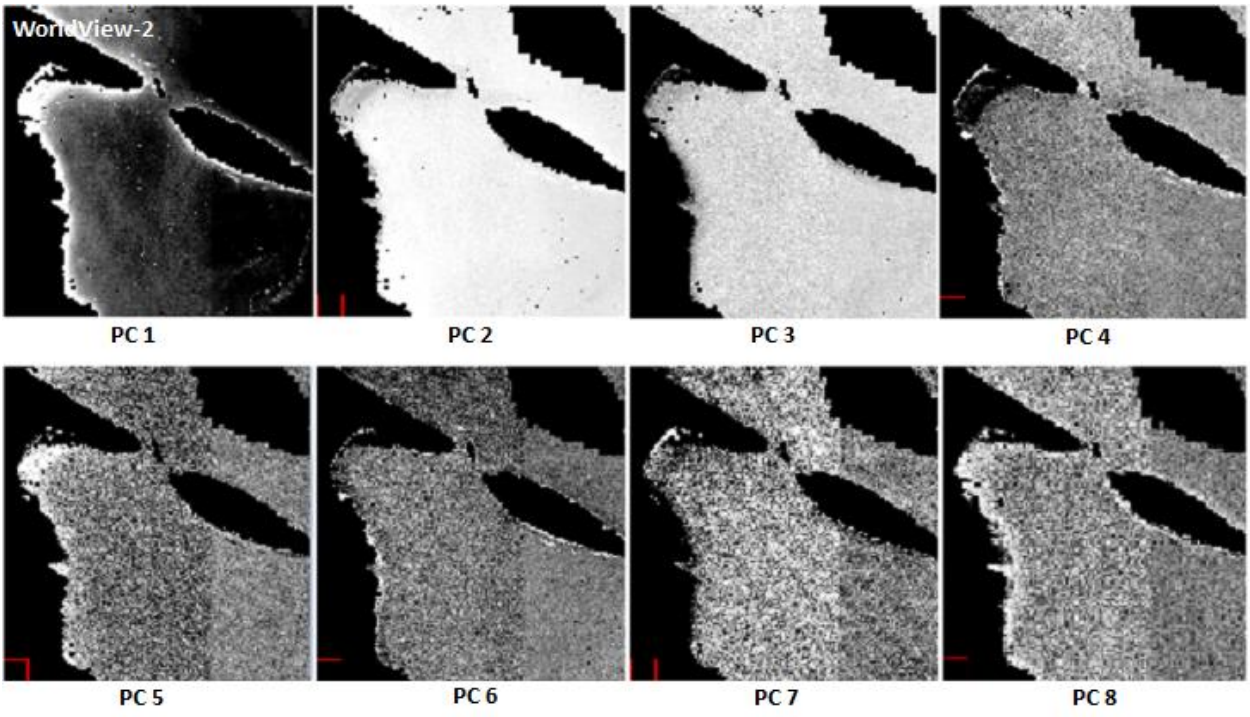


**Appendix B – Band images for each PC band resulting from principle components analysis (PCA) of the SPOT-6 image.**

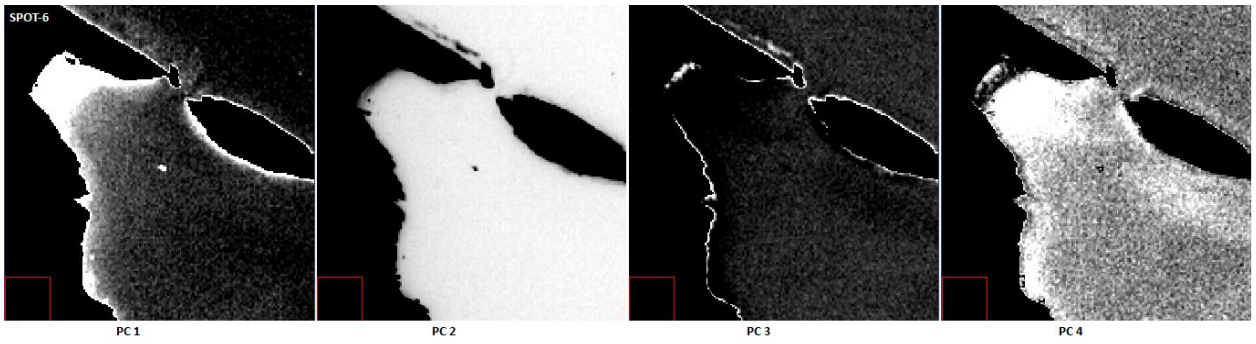

**Appendix C – M-statistic results for complete set of WorldView-2 spectral variables, including reflectance bands, reflectance band ratios, and PC bands. The greatest M-statistic value for each kelp-substrate pair is identified with a black box.**

| | | M-statistic between kelp and: | | | | |
|---|---|---|---|---|---|---|
| | spectral variable | sand | eelgrass | green algae | deep water | whitecap |
| Reflectance variables | CB | 0.3 | 0.2 | 0.6 | 0.9 | 0.5 |
| | B | 0.6 | 0.8 | 1.3 | 0.8 | 0.6 |
| | G | 0.8 | 1.3 | 1.9 | 0.8 | 0.7 |
| | Y | 0.7 | 0.8 | 1.4 | 1.5 | 0.5 |
| | R | 0.5 | 0.5 | 1.2 | 1.4 | 0.5 |
| | Re | 0.1 | 0.7 | 0.1 | 2.7 | 0.6 |
| | N1 | 0.2 | 0.5 | 0.0 | 2.9 | 0.8 |
| | N2 | 0.0 | 0.3 | 0.1 | 2.6 | 0.7 |
| Reflectance band ratio variables | CB:B | 0.5 | 0.3 | 0.4 | 0.3 | 0.3 |
| | CB:G | 0.8 | 0.6 | 0.7 | 0.1 | 0.4 |
| | CB:Y | 1.2 | 0.5 | 1.1 | 0.1 | 0.1 |
| | CB:R | 1.1 | 0.4 | 0.9 | 0.1 | 0.2 |
| | CB:RE | 0.2 | 0.8 | 0.5 | 0.4 | 1.5 |
| | CB:N1 | 0.3 | 0.7 | 0.6 | 0.3 | 1.6 |
| | CB:N2 | 0.1 | 0.4 | 0.4 | 0.4 | 1.3 |
| | B:G | 0.6 | 0.4 | 0.6 | 0.1 | 0.3 |
| | B:Y | 0.7 | 0.1 | 0.6 | 0.2 | 0.4 |
| | B:R | 0.5 | 0.1 | 0.2 | 0.2 | 0.2 |
| | B:RE | 0.6 | 1.3 | 1.0 | 0.4 | 1.6 |
| | B:N1 | 0.6 | 1.3 | 1.1 | 0.3 | 1.8 |
| | B:N2 | 0.5 | 1.0 | 1.0 | 0.4 | 1.4 |
| | G:Y | 0.0 | 0.9 | 0.5 | 0.3 | 0.7 |
| | G:R | 0.2 | 1.1 | 0.8 | 0.3 | 0.8 |
| | G:RE | 0.9 | 2.0 | 1.4 | 0.4 | 1.6 |
| | G:N1 | 0.9 | 2.0 | 1.5 | 0.3 | 2.0 |
| | G:N2 | 0.8 | 1.7 | 1.6 | 0.4 | 1.5 |
| | Y:R | 0.3 | 0.5 | 0.4 | 0.7 | 0.1 |
| | Y:RE | 0.8 | 2.1 | 1.6 | 0.3 | 2.0 |
| | Y:N1 | 0.8 | 1.9 | 1.6 | 0.3 | 1.6 |
| | Y:N2 | 0.7 | 1.6 | 1.7 | 0.4 | 1.6 |
| | R:RE | 0.7 | 1.8 | 1.4 | 0.3 | 1.6 |
| | R:N1 | 0.8 | 1.6 | 1.4 | 0.3 | 2.3 |
| | R:N2 | 0.7 | 1.2 | 1.4 | 0.3 | 1.5 |
| | Re:N1 | 0.4 | 0.5 | 0.0 | 0.1 | 0.1 |
| | Re:N2 | 0.7 | 1.3 | 0.4 | 0.5 | 0.1 |
| | N1:N2 | 0.9 | 1.1 | 0.6 | 0.9 | 0.1 |
| d vari | PC1 | 0.6 | 0.3 | 0.5 | 2.8 | 0.2 |
| | PC2 | 2.5 | 1.1 | 0.8 | 1.5 | 1.1 |

| | | | | | | |
|---|---|---|---|---|---|---|
| | PC3 | 1.7 | 0.3 | 1.3 | 0.2 | 0.0 |
| | PC4 | 2.6 | 1.7 | 0.6 | 1.8 | 1.0 |
| | PC5 | 1.4 | 1.8 | 0.4 | 1.9 | 0.9 |
| | PC6 | 1.5 | 1.5 | 0.2 | 1.9 | 1.4 |
| | PC7 | 0.1 | 0.6 | 0.0 | 0.9 | 0.5 |
| | PC8 | 1.0 | 0.8 | 0.8 | 0.7 | 0.3 |

**Appendix D – M-statistic results for complete set of SPOT-6 spectral variables, including reflectance bands, reflectance band ratios, and PC bands. The greatest M-statistic value for each kelp-substrate pair is identified with a black box.**

| | spectral variable | M-statisic between kelp and: | | | |
|---|---|---|---|---|---|
| | | **sand** | **eelgrass** | **green algae** | **deep water** |
| Refl bands | B | 1.7 | 1.1 | 6.5 | 1.5 |
| | G | 1.9 | 0.9 | 7.9 | 1.2 |
| | R | 1.4 | 0.2 | 11.2 | 1.1 |
| | NIR | 0.9 | 1.7 | 7.5 | 2.3 |
| Refl band ratios | B:G | 0.9 | 0.7 | 0.9 | 1.0 |
| | B:R | 2.1 | 1.9 | 1.6 | 1.7 |
| | B:NIR | 2.4 | 1.3 | 1.2 | 2.8 |
| | G:R | 1.4 | 1.6 | 1.2 | 2.1 |
| | G:NIR | 2.7 | 1.1 | 0.7 | 5.2 |
| | R:NIR | 2.2 | 1.1 | 0.0 | 4.0 |
| PC bands | PC1 | 1.7 | 0.7 | 9.5 | 0.7 |
| | PC2 | 0.5 | 1.8 | 7.9 | 2.3 |
| | PC3 | 1.9 | 1.2 | 1.2 | 1.5 |
| | PC4 | 0.6 | 1.0 | 1.1 | 1.2 |

**Appendix E. Band images of each selected spectral variable in the Case 1 and Case 2 selected variable sets of WorldView-2. Area shown is Georgeson Island, which appears in black due to land mask. Note the kelp bed circled in red and its contrast from the rest of the cover classes in the image (aside from the land mask).**

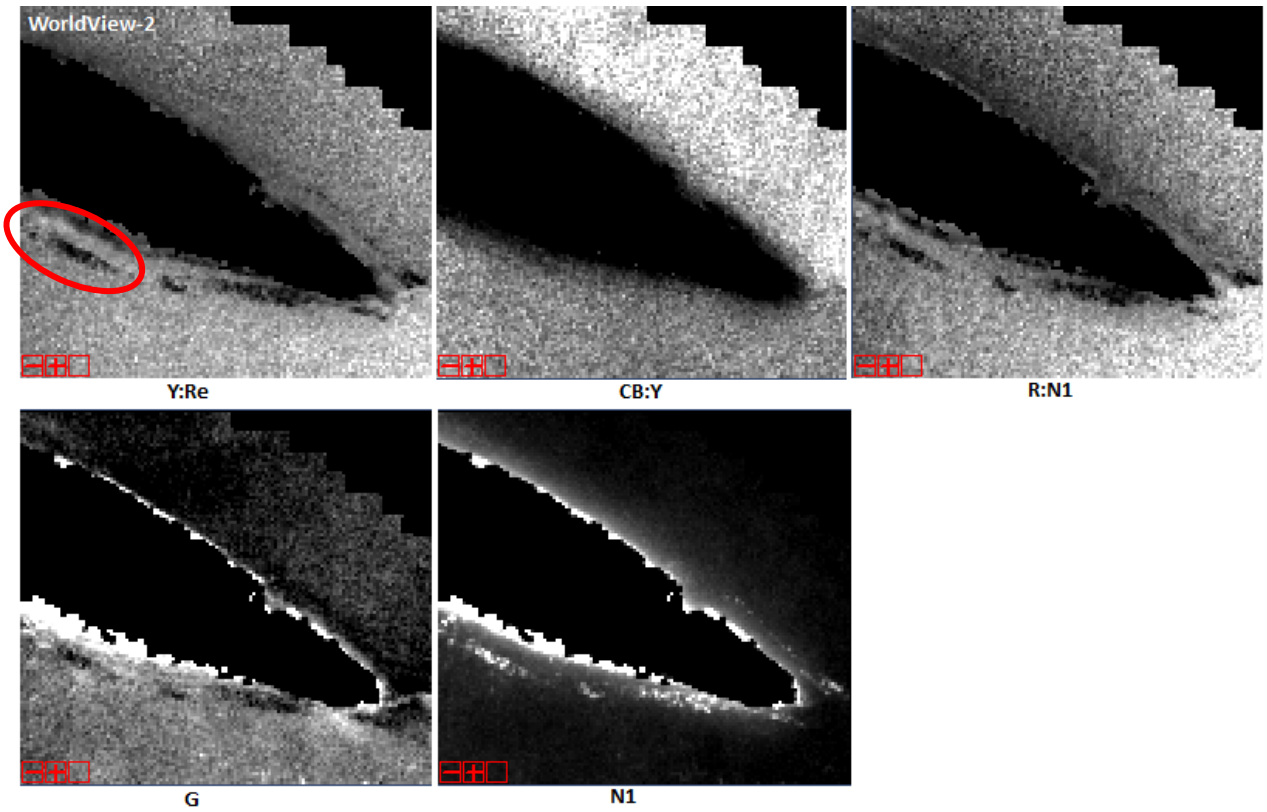


Case 1

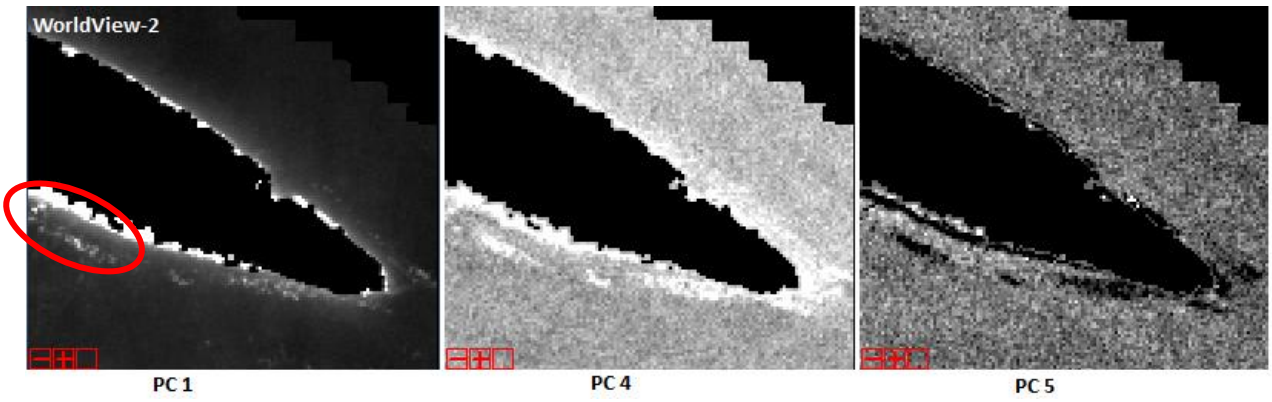


Case 2

**Appendix F. Band images of each selected spectral variable in the Case 1 and Case 2 selected variable sets of SPOT-6. Area shown is to the south west of Georgeson Island, which appears in black due to land mask. Note the kelp bed circled in red and its contrast from the rest of the cover classes in the image (aside from the land mask).**

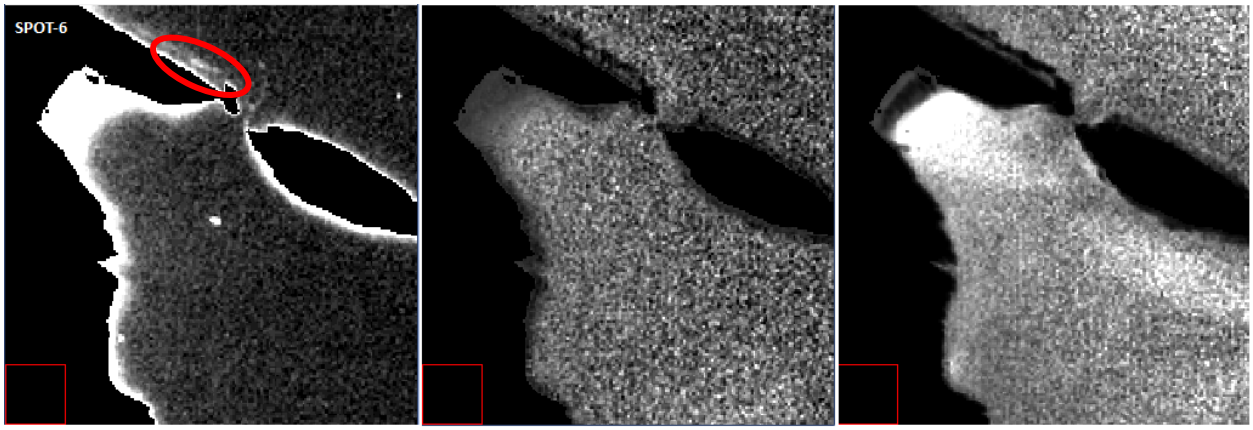


Case 1

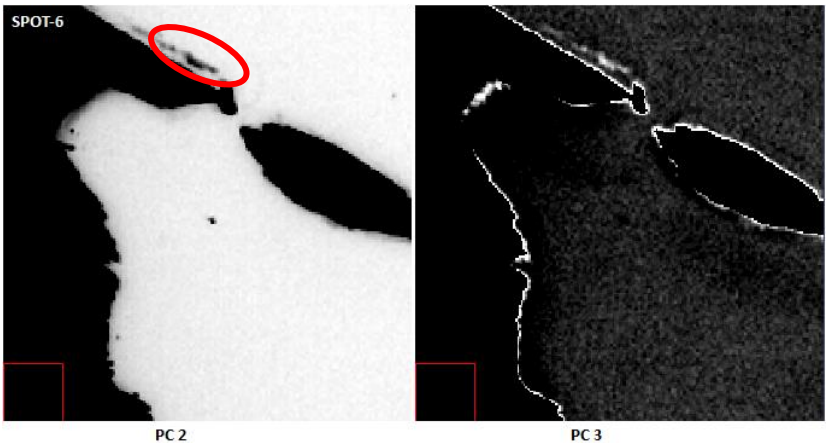


Case 2